AALBORG UNIVERSITY
STUDENT REPORT

Evaluation of Basic Preprocessing, aCompCor and FSL FIX for Optimal fMRI Preprocessing in an Individual Differences Study Perspective

3nd semester Masters, Biomedical Engineering & Infomatics - Fall 2018

Project group: 19gr9411

Christian Korfitz Mortensen, Martin Alexander Garenfeld

ii

Preface

Morbi luctus, wisi viverra faucibus pretium, nibh est placerat odio, nec commodo wisi enim eget quam. Quisque libero justo, consectetuer a, feugiat vitae, porttitor eu, libero. Suspendisse sed mauris vitae elit sollicitudin malesuada. Maecenas ultricies eros sit amet ante. Ut venenatis velit. Maecenas sed mi eget dui varius euismod. Phasellus aliquet volutpat odio. Vestibulum ante ipsum primis in faucibus orci luctus et ultrices posuere cubilia Curae; Pellentesque sit amet pede ac sem eleifend consectetuer. Nullam elementum, urna vel imperdiet sodales, elit ipsum pharetra ligula, ac pretium ante justo a nulla. Curabitur tristique arcu eu metus. Vestibulum lectus. Proin mauris. Proin eu nunc eu urna hendrerit faucibus. Aliquam auctor, pede consequat laoreet varius, eros tellus scelerisque quam, pellentesque hendrerit ipsum dolor sed augue. Nulla nec lacus.

Contents

Part I

Problem Analysis

1 | Introduction

To experience and live with chronic pain can be immensely debilitating for any individual, and the consequences of experiencing chronic pain has been linked to numerous physical and mental conditions: restrictions in mobility and daily activities, dependency of therapeutic drugs, anxiety and depression and a reduction in quality of life [1, 2].
More than 100 million Americans are estimated to live with chronic pain, manifesting an extraordinary amount of human suffering along with additional large economic societal expenditures, as cost of medical care and loss of wages and productivity are escalating [3, 4]. Compared to other major health conditions the number of patients suffering from chronic pain outnumber the combined total of patients suffering from heart disease and stroke, diabetes and cancer, and these conditions often include pain as a contributing component [2].
"An unpleasant sensory and emotional experience associated with actual or potential tissue damage, or described in terms of such damage", is how the International Association for the Study of Pain defines pain [5]. The phenomenon of pain is a very complex composition of both psychological factors, personality traits and states, and cognitive, emotional, motivational, contextual and cultural variables. Pain can furthermore be defined either acute or chronic. Acute pain is a healthy response making up a self defense mechanism to warn and protect the human organism from any potential or further harm. [6, 7, 4] Contrary to acute pain, chronic pain is not linked to organ damage of any kind, and therefore does not serve any useful purpose to the human organism [8].
It still remains incredibly challenging to assess and treat pain, as the mechanisms during the experience of pain is not yet fully understood [9, 10]. This includes all neurological steps in the processing of pain - from the peripheral detection of a stimulus to the spinal cord transmission and brain processing, including the further relay of the pain experience [11]. A step towards getting a higher understanding of chronic pain is to examine the mechanisms involved in acute pain. A justification for this reasoning is that chronic pain often is transitioned from repetitive acute nociceptive stimulations that leads to neuroplastic changes. [11, 12]
Multiple studies [13, 14, 15, 4] have shown that the perception and sensitivity to acute pain are disposed to a great extent of subjective variability, suggesting that a pivotal key in understating the brain mechanism during noxious stimuli is found in the individual differences between subjects. Additionally, an individual's sensitivity can vary substantially from day to day, despite being exposed to the same stimuli, and the psychophysical rating given by the patient can rather looked upon as artifact in the various scales used for reporting, than actually reflecting an unbiased measure of the experienced pain. It can furthermore be difficult for the physician to evaluate the patient's experienced pain from a third-person perspective. [13]
To examine if there is a difference between individuals in brain activation during the experience of pain and if this activation is correlated with the self-reported experience of pain is therefore of great interest. [13]

2 | Problem Analysis

In the problem analysis chapter a theoretical overview of essential topics encapsulating the study of pain will be presented. First, the mechanisms involved in the experience of pain will be described, and how the metabolic response of brain activation can be translated into images. Subsequently, differences in the experience of pain between individuals will be outlined, along with the possible difficulties in interpreting the corresponding images. Lastly, different methods to counter these difficulties will be presented, thereby laying the foundation for understanding the problems faced when studying the differences in the individual's experience of pain.

2.1 Processing of Pain in the Nervous System

Pain is a complex subjective phenomenon, where sensory and affective components along with cognitive elements are activated to refrain an individual from further and future similar damage [4].
When the body is exposed to noxious stimuli, whether it originates from external or internal afflictions, information about the damaging stimuli is transmitted through neural pathways and through the peripheral nervous system to the autonomic and central nervous system. This relay to the brain of a damaging event is called nociception. It is mediated by certain receptors called nociceptors, which are attached to myelinated Aδ and unmyelinated C fibers that terminate at the dorsal horn of the spinal cord. Perception of pain occurs when stimulation of nociceptors is high enough to activate Aδ fibers, which results in an acute experience of prickling pain. When the stimulation increases, C fibers are activated, which results in a more intense pain experience that remains after the stimulus has ceased. These two phases of pain experience are associated with acute noxious stimulus, where the first phase is referred to as fast pain, and is of moderate intensity and appears immediately after the stimulus. The second phase, which is known as slow pain, is not as localizable, appears after a longer delay and is more painful. Activation of nociceptors can happen from sufficiently intense mechanical, chemical or thermal stimulation. Nociceptor activation is also modulated by inflammatory and bio-molecular influences. However, it is also possible for individuals to experience pain without a measurable noxious stimulus and for individuals to undergo a damaging trauma without suffering any pain sensation. [7]
As stated in The International Association for the Study of Pain's definition of pain, not only somatosensory components are involved in the experience of pain, but also cognitive and emotional elements. Psychological processes are major elements in the perception and expression of pain and involve the individual's attention to the painful infliction, the cognitive appraisal of pain and emotional and behavioral reactions. These factors may have increasing or decreasing effects on the perception of pain.
As mentioned, the activation of nociceptors is transmitted along axons in peripheral nerves to the dorsal horn of the spinal cord. From here the information is sent up the spinal cord

via the spinothalamic tract to the thalamus. The thalamus functions as a major transmission location for sensory information to the cerebral cortex. The neural pathways terminate in subdivisions of the thalamic nuclei, from where the information is relayed to different cortical and subcortical divisions, including regions of the cerebral cortex, amygdala, hypothalamus, periaqueductal grey and basal ganglia. Worth remarking is that the insula and anterior cingulate cortex seem to almost always be activated when nociceptors are stimulated. [16, 4] Figure 2.1 depicts the anatomy of pain pathway propagation of neurological signal from nociceptor to spinal cord to the brain centers affiliated with pain reception and modulation.

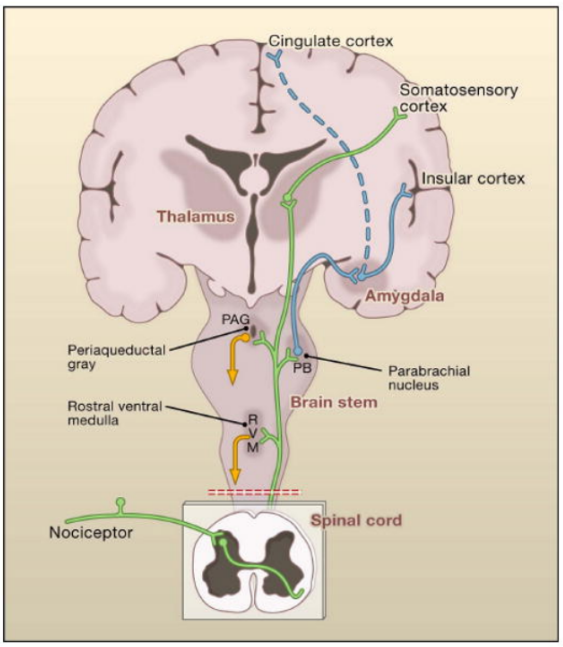

Figure 2.1: Coronal view of the mechanisms and regions associated with the experience of pain. The pain pathway from nociceptive input propagating through the dorsal horn continuing up through spinal cord to the affiliated brain regions. [17]

These structures are what process somatosensory input and is outputting neural activation that affects nociception and pain perception. [7] This means that the brain does not only passively receive sensory input, but in addition actively regulates the sensory transmission by influencing the dorsal horn of the spinal cord through a descending modulation. The brain structures involved in this regulation include the same as mentioned along with the rostral ventromedial medulla and dorsolateral pons/tegmentum. [16] Thus, when determining the intensity of pain perception during noxious stimulus of an individual these brain structures are of great importance to examine.

2.2 Metabolic Response to Brain Activation

To further understand the origin of brain activation during the experience of pain and how this activity is modulated by the brain, a measure of brain activation is therefore needed. To get a measure of brain activation, the underlaying physiologic response is therefore of great importance to understand.
The activation of a brain region starts with a neurological input containing information about the noxius stimuli [16]. The increased neurological activity effects local metabolism as processing of the signal requires adenosine triphosphate (ATP) consumption during e.g. the reception and reformation of the action potential. Thus, ATP starts to be processed, leading to a decrease in oxygen concentration and increase in waste products. Thereby, the metabolic need for oxygen increases. Subsequently, these factors present in the local tissue of the corresponding brain region activate a vasodilation, increasing the blood flow to that region to reestablish the local homeostasis. During this regulation a not yet fully understood phenomenon occurs as more oxygenated blood than needed to compensate for the offset is delivered. Thereby flooding the local region with oxygenated blood. This response to the increased neural activity is known as the hemodynamic response. The overall increase in neural activity in that specific region following the need for metabolic regulation thereby permits the measure of the hemodynamic response, hence becoming an indirect measure of the neural activity. An example illustrating the hemodynamic response can se seen in figure 2.2. [18, 19].

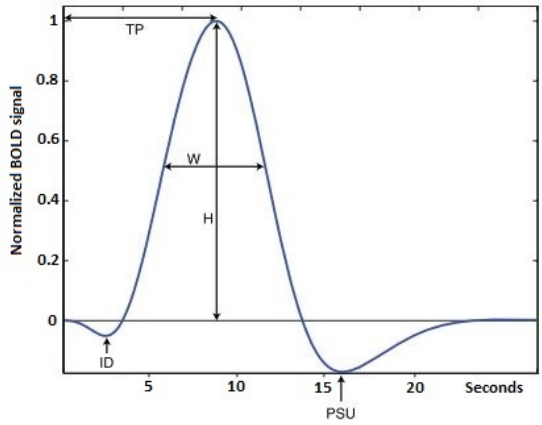

.

Figure 2.2: A depiction of a single hemodynamic response curve. ID is the initial dip as less oxygen will be present as the metabolic demand increases, TP is time from stimulus until peak, W and H is the width and height of the response and PSU is a post stimulus undershoot. Modified from [19]

Figure 2.2 should be considered the perfect noiseless hemodynamic response curve, to a brief stimuli, though the reality is that the response is effected by physiologic noise parameters and would be delayed in time compared to the stimuli onset. The peak height of the curve is commonly the most interesting feature of the response, as it portrays the amount of neural activity. The time to peak will occur 4-6 seconds after stimulus onset.

The duration of a response is around 20 seconds. There will further be a noticeable initial dip of 1-2 seconds duration, when the initial oxygen reserves are used up and a 20 second poststimulus undershoot as homeostasis is reestablished. [19]

2.3 Imaging of Brain Activation

The metabolic changes associated with the hemodynamic response can be accentuated through the use of fMRI [18]. The following section will introduce the concept of fMRI and why it can be used to study brain activation. Before reading this section, it is assumed that the reader is familiar with basic physics of nuclear magnetic resonance imaging and image reconstruction. If not, an overview can be found appendices A.1 and A.2.
The fundamental reason behind why fMRI can be used to study brain activity relies on the indirect measure of the magnetic properties of blood. MRI is dependent on susceptibility, which is the extend to which a material can be affected by magnetization. Local changes in susceptibility results in changes in the MR signal. [20] Changes in susceptibility arise with the hemodynamic response as oxygenated hemoglobin (HbO_2) is diamagnetic, and de-oxygenated hemoglobin (Hb) is highly paramagnetic due to its four unpaired electrons, resulting in what is known as the Blood Level Oxygen Dependent (BOLD) contrast. Thus, as presented in the prior section, the increase in neural activity increases the blood flow to an extend greater than the metabolic utilization of oxygen, which results in a high (HbO_2) to (Hb) ratio. This makes up the difference in BOLD contrast. [18, 19, 21] Figure 2.3 illustrates how the BOLD contrast is dependent on the amount of oxygenated hemoglobin.

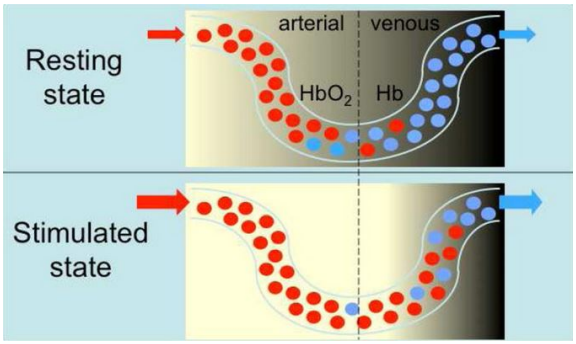

Figure 2.3: Illustration of the concentration difference in oxygenated (HbO_2) and de-oxygenated hemoglobin (Hb) during resting state and stimulated state. The diamagnetic properties of oxygenated blood changes the local magnetic substitutability facilitating a greater contrast change. [18]

The changes in the BOLD contrast can be recorded by using a T_2^* sequence, which is sensitive in detecting changes on the magnetic field [21, 22]. The areas highly filled with oxygenated blood will result in a higher signal in the T_2^*-weighted sequence making these appear brighter in the reconstructed image. To capture the changes in blood flow over time the acquisitions has to be relatively fast. To achieve fast sequences, the result is a sacrifice of spatial resolution for temporal resolution, making it possible to acquire a

whole brain volume in a couple of seconds. [21]
Other methods, as the arterial spin labeled (ASL) method exist for accentuating the functionality of the brain, but BOLD is favored, because it offers a high contrast to noise ratio and it is relatively simple to implement. [22]
As fMRI can capture the neurological response to pain through the hemodynamic response a measure to study the individual's response to pain is thereby derived. To know more of how the individual's perception of pain is measured in general and by fMRI, including the current difficulties, is of great significance.

2.4 Individual differences in pain perception and fMRI

The study of individual differences is basically to examine how each individual respond to the same intervention. This has been of great interest in medical fields ranging from psychology to pain research, as an understanding of each individual would shape more precise treatments given the individual's unique characteristics. However, understanding why individuals react differently across sensory modalities has for long been a perplexing problem. In pain research, studies have shown that individuals report a large difference in pain sensitivity on a Visual Analogue Scale (VAS), when exposed to identical noxious stimuli [9, 13]. This could indicate that individuals have different neurological responses to the same noxious stimuli, but on the other hand raise questions about the individual: is the subject over/underplaying the pain experience or engaging in drug seeking behavior? Thus, in the treatment of pain it has been of great interest to examine if the subjectively reported pain experience correlates with the actual neurological response in the individual. [10] Verifying a correlation between self-reports and brain activity during evoked pain stimulus would function as a important step in improving physician's understanding and treatment of patients suffering from chronic pain. Brain imaging could on sight be an assistive tool to self-reports and behavioral evidence when assessing a patient's claim regarding pain and physical condition. Such an addition would serve an especially valuable function when assessing patients unable to communicate verbally (e.g. young children and patients with dementia), patients with self-reports and behavioral evidence that are conflicting and for personalized pain management. In perspective, as brain imaging gets more accepted in personalized pain management it will gain more interest in legal practices. Using it as proof or disproof on whether a patient is actually experiencing pain might affect financial outcome in insurance cases. However, due to ethical and jurisdictive circumstances it would be inappropriate to use it as a tool in such cases until it has been sufficiently verified. [4]
An indirect measure of functional brain response can be achieved through a BOLD fMRI scanning, and is often used to get a generic understanding of brain function in research. Averaging data across individuals is commonly applied to raise the signal-to-noise ratio (SNR). However, while providing a general knowledge on brain function, this practice excludes the possibility of observing brain function in the individual. The interest of examining individual differences in brain activity has been present for several years, but

the technology has only during recent years been advanced enough for it to be carried out, due to higher magnetic field strength and faster acquisition time. [23]
In 1999 and 2003 Coghill et al. [24, 13] published studies showing correlation between intensity of activation of specific brain regions associated with processing of noxious stimuli and subjects' subjective pain sensitivity. Positron Emission Tomography (PET) scans and BOLD fMRI in a 1.5 tesla scanner was used respectively in the two studies for functional brain mapping. However, as Dubois et al. [23] emphasize only during the recent years the MRI technology has been advanced enough to create images with sufficient SNR to use as means in studying individual differences. A review study by Wood et al. [25] comparing 1.5 tesla and 3.0 tesla scanners, showed that using the BOLD fMRI technique can produce better susceptibility contrast sensitivity and due to the naturally higher SNR in 3.0 tesla scanners a 40 percentage increase in activation detection can be generated.
In that relation, a validation of the 2003 study by Coghill et al. [13] with data from a 3.0 tesla scanner would be relevant, as a 1.5 tesla scanner was used for BOLD fMRI acquisition in [13]. Further reasoning for a validation study is that clinics tend to get higher tesla scanners installed, when desiring to get finer images in fMRI [25]. Thus, the future of fMRI lies within the use of higher tesla scanners. In [13], a total number of 17 subjects were included. To raise the reproducibility and verification in a validation study the number of participants included should be increased to examine if statistically significant result can be found in a higher sample size [23, 26].
However, a downside of 3.0 tesla scanners compared to 1.5 tesla scanners is that artifacts related to motion, respiration, bloodflow, pulsation of cerebrospinal fluid and air-tissue interfaces are more prominent [25].

2.5 Artifacts Associated with BOLD fMRI

When BOLD fMRI sequences are used to detect brain activity during in vivo experiments, not only task related activation will be present. Unfortunately, in most experiments sources of noise will inevitably impact the scan. [27]
As BOLD fMRI relies on very precise temporal and spatial placement, even millisecond or millimeter fluctuations caused by motion can have a large impact on the quality of the acquired signal. Motion does not only distort the brain in space but also disrupts the formation of the magnetic gradients that enables the BOLD signal to be detected correctly. Bulk motion of the head will cause the content of each voxel to change. As the maximum value of net magnetization in the direction of the magnetic field (M_0) is directly proportional to the number of spins in that voxel the BOLD signal will consequently be altered. In tissue interfaces such as white/grey matter boundaries, at the edge of the brain and around large vessels this is especially an issue. Furthermore, bulk motion will change the uniformity of the magnetic field as is has been tuned for a particular head position. This also directly affects M_0 and results in dropouts, reductions in signal intensity, in the BOLD signal and thus in the subsequent readout. Lastly, movement will change steady state magnetization, by changing the time between excitations in the tissues that have moved from a slice to another. M_0 is affected until steady state has been reached again, and is referred to as the spin history effect. The spin history effect can cause the intensity

of the BOLD signal to be detected as twice the level of the expected signal. [28] This will often result in an image where the intensities change in a striped pattern [19].
A typical protocol in pain research involves inducing noxious stimuli on the participant while recording the brain activity. These stimuli often causes the participant to move even more. During the movement some brain regions might also show activation associated with stimulus. Therefore it is easy to mistake brain activation with stimulus correlated movement when analyzing the data, resulting in a weaker or even false statistical analysis. [19]
Motion due to cardiac and respiratory cycles will cause the same artifacts as during bulk motion of the head. Additionally, cardiac pulsation and respiratory cycles will cause the brain stem to push the surrounding brain tissue. This will cause deformation and movement of cerebrospinal fluid that will form changes in M_0. Further artifacts can be found related to the frequency content of cardiac and respiratory cycles. The frequency of cardiac and respiratory cycles at rest are around 1 Hz and 0.3 Hz respectively. Relatively high-frequent compared to the BOLD signal of < 0.1 Hz. As the repetition time in a BOLD fMRI usually is 2-3 seconds, parts of the cardiac and respiratory cycles will be aliased into the BOLD signal's frequency bandwidth. Thus, these artifacts can be mistaken for the BOLD signal when examining the frequency content. Another respiratory factor that affects the BOLD signal is the arterial level of CO_2. It works as a vasodilator and facilitates a global increase in the cerebral blood flow and thereby the BOLD signal. Thus, when a participant holds the breath hypercapnia arises and the BOLD signal increases, and during hyperventilation hypocapnia arises causing a decrease in the BOLD signal. [28] This type of artifact might occur more when the participant is being subjected to noxious stimuli to attenuate the pain experienced.
Furthermore, artifacts can form in areas where air and tissues meet, e.g. sinuses and the ear canals, and is caused by the main magnetic field inhomogeneities the air-tissue interface produce. It will be visualized as dropouts in the brain region adjacent to the air-tissue interface. [19]
It can be summarized that many sources of noise can alter and disguise the signal of interest. Thus, being able to separate signal sources from noise is of great importance before analysing BOLD fMRI data, to avoid making any conclusions based on spurious data.

2.6 State of the Art in MRI Preprocessing

In section 2.5 the various types of corrupting noise was presented. Continuous efforts have been made to avoid, remove and limit the influence of artifactual contributors before the quantitative fMRI analysis. Regular preprocessing methods of motion correction, spatial smoothing and temporal filtering, have for long been a part of the preprocessing toolbox [19]. But as studies grow more complex, seek greater SNR and introduce greater noise sources associated with the newer scanners, the need for more complex and fitting cleanup tools to add to the preprocessing toolbox is present. [25, 29]
In noise removal of fMRI datasets, there are mainly two widely used approaches: one data driven and one model based [27, 30]. In the latter, acquired data is compared to a

predefined model, such as in the general linear model. These methods include additional physiological recordings, e.g. heart rate and breathing cycle, and use these regressors of non interest to regress/filter out their contribution to the recorded fMRI dataset. [27, 30, 31] Data driven models instead draw upon the data within the dataset utilizing methods of principal component analysis (PCA) and independent component analysis (ICA). Data driven methods are ideal when no good existing model fits the data as they can analyze the data in more flexible way. Hence, they are able to identify new and unexpected noise components, which then can be made to fit the model, thereby laying the foundation for a model based noise removal. [30]
One of the most often referred to articles making use of a model based method is the RETROspective Image CORrection (RETROICOR), introduced by Glover et al. [32]. By measuring the phases of respiratory and cardiac cycles and comparing these to the fourier terms of the fMRI scan, they showed that it was possible to find these physiologic noise contributions which was synchronized with the scan. These could then be out-filtered showing considerably lowered peaks in the frequency spectrum at 0.8 Hz for cardiac influence and 0.15 Hz for respiratory influence. [32]
A limitation of the model based RETROICOR was its dependency on physiologic data being acquired from external devices. A study by Behzadi et al. [33] surpassed this restriction by utilizing a proposed data driven model of Component based noise Correction (CompCor). Instead of relying on data from external measurement of physiological noise, the CompCor method uses a PCA derived from noise regions of interest (ROI) to describe the physiological noise. Two methods of determining noise ROI's were introduced: one using anatomical data to identify voxels where no neurological activity is presumed, such as in white matter and cerebrospinal fluid (CSF), the other defining noise ROI's from voxels with high temporal standard deviation (tSTD) as these were found to correspond to ventricles, edge-regions, and vessels. The first five components from the PCA were hypothesized to describe the variance of the noise, and were used to fit a general linear model as nuance regressors and thereby remove the noise influence. Both CompCor methods produced a significant reduction in physiological noise fluctuations compared to the RETROICOR for BOLD fMRI. In addition, the second CompCor method was able to reduce subject motion artifacts. Though in cases of both severe motion artifacts and physiological fluctuations the PCA might only be able to describe one of the factors, limiting its use. [33]
Model based noise cleanup methods like RETROICOR depend on external physiological measurements, and both the PCA based method CompCor and RETROICOR mainly focuses on physiological noise. This suggest that methods which can incorporate a higher level of motion correction along with correction for MRI scanner artifacts might be of greater use.
ICA is another data driven model, building on the blind source separation paradigm, for source analysis of fMRI datasets and was first introduced in 1998 by Mckeown et al. [34]. Since then, multiple studies [35, 36, 37, 38, 39] have used and developed the use of ICA further. ICA has proven to be a powerful tool in separating the different sources which in summation comprise the complete fMRI scan. By maximizing spatial independence and non-gaussianity, the data can be decomposed into components each consisting of an

activation map and its corresponding time course. [27] This facilitated the prospect of by visually inspecting the components, a discrimination between artifactual activation and task-related could be made. Tools for easy employment of the ICA has been presented by groups like the Oxford University Centre for Functional MRI of the Brain (FMRIB), who presented a program called MELODIC for fast ICA implementation. [40] The possibility of visually inspecting and labeling components as either artifactual or of interest, lead to discussions on standardization and comparability, as labeling of components could be subjected to operator biasing. Studies in the likes of [27, 41], have proposed ways to recognize different artifactual components, but these can be hard to utilize since every component will be different from another. Subsequently, automatic labeling algorithms have been made to increase the sensibility, reliability and reproducibility of fMRI studies. These have been made by training classifiers in recognizing and separating artifactual components. [39]
In 2014 Salimi-Khorshidi et al. [27] introduced the FMRIB's ICA-based X-noiseifier (FIX), for automatic denoising of resting state and task-related fMRI data. This methods employ the use an initial standard processing followed by a spatial-temporal fastICA, hand labeling of training set, feature extraction of 180 features and a heracial classifier for classification. [27]
The use of pattern recognition is an interesting proposal as it makes way for a standardized approach, and reduces the labor intense work of labeling all components.

3 | Study Objective

In summary it would be beneficial for the understanding of chronic pain to gain further knowledge on the brain mechanisms associated with acute pain. As different individuals report a wide variety in pain sensitivity when given identical pain stimuli, an examination on if the subjective reports correlate with intensity in brain activation in brain regions associated with pain would be of high interest. When using 3.0 tesla MRI scanners to indirectly measure brain activity through BOLD fMRI sequences, more of the activity will be captured compared to using 1.5 tesla scanners. The images will on the other hand be more prone to contain noise. For this reason proper preprocessing is needed to separate noise from signal of interest before analysing the images. During the recent years more preprocessing methods have been developed in the field of fMRI as alternatives to the standard method. These methods include the CompCor and the FSL FIX. A comparison of these newer methods and the standard method on a large set of subjects would be favorable in the field of pain research using fMRI, as this could provide insight on the advantages/disadvantages of each preprocessing method. This introduces the study objective:

Compare and evaluate the performance of standard preprocessing, CompCor and FSL FIX for noise removal in images acquired with BOLD fMRI studying individual subjects' brain activation to noxious heat stimuli.

Part II

Problem Solution

4 | Methods

The methods section serves purpose of presenting the study design, how the test data was acquired and document the implementation of the three preprocessing methods used for noise removal. First, a flowchart introducing an overview of the general processing pipeline will be given, see figure 4.1. Afterwards, the data acquisition protocol and the subjects demographics will be presented. Subsequently the implementation of the standard preprocessing methods will be introduced, followed by the FSL FIX method. Finally, the statistical framework used for testing the performance of each preprocessing method is presented.

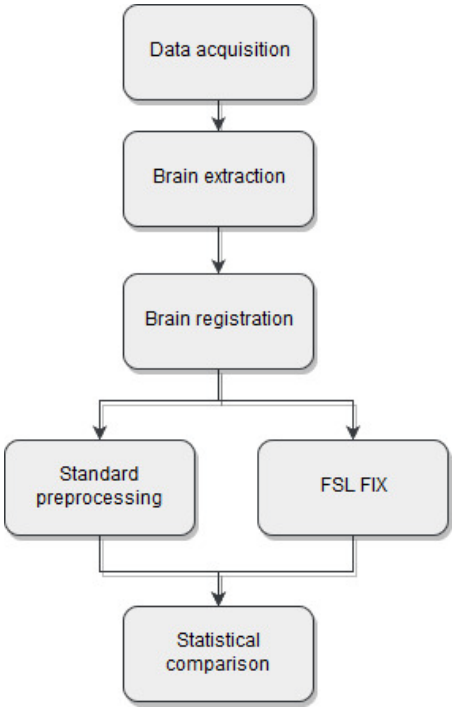

Figure 4.1: Flowchart presenting an overview of the processing pipeline throughout the methods chapter. Initially the data is acquired and the brain is segmented and extracted from both a structural and functional scan. Afterwards the extracted brains are registered to each other and to a standard. Then the brain from the functional scan is run through the pipeline of each of the two preprocessing methods, and subsequently the results of noise removal from each pipeline is compared.

4.1 Study Protocol

The data used in this study originates from an ongoing Individual Differences Project (IDP) at the Department of Anesthesia at Cincinnati Children's Hospital and Medical Center. In this section, information on the study design will be outlined, i.e. which criteria that were set for in/exclusion, what the stimuli design was and how the data was acquired. The IDP study design involved subjecting the participant to several types of

noxious stimuli. Though for the scope of this project, only the heat stimuli design will be described.

Healthy subjects between 14 and 44 of age were recruited with no discrimination of gender and ethnicity. INFORMATION ON MEAN AGE AND STD OF THE PARTICIPANTS. As the study involved MRI scanning, subjects suffering from claustrophobia or had any electronic or metallic implants were not able to participate. Further exclusion criteria were pregnancy, skin conditions or past skin damage on or near the site of the heat stimuli delivery and intake of medications that may alter pain sensitivity or brain activation. The participants were able to withdraw from the study at any time. Additionally, the study investigators were able to withdraw participants if the they declined to comply with the experiment protocol, if a drug or pregnancy test showed positive, if there was an identification of severe brain, neurological or psychological abnormalities occurred or if the investigator assessed that it would be in the participant best interest.
Before enrollment in the study, the participants received a consent document (including the guardians/parents for participant under 18). First when full comprehension of the information was demonstrated the participant and guardians/parents would sign the document.

Data acquisition

The heat stimuli was delivered on the calf of the left leg with the Pathway stimulator[1], while the participant was placed in a MRI scanner for recording of brain activity. For visualization of brain structures and spatial normalization of functional data high resolution T_1-weighted structural scans were first obtained. MENTION WHICH EXACT SEQUENCES THAT WERE USED (MAKE A TABLE WITH THIS INFORMATION). Each participant went through three different heat stimuli runs with seven noxious heat stimuli in each. Each heat run had a unique sequence of 10 seconds of noxious stimuli temperatures of 47°C or 48°C interleaved with resting periods of skin temperature (35°C) stimuli. The design of the three heat runs can be seen in figure 4.2. Following each noxious stimulus the participant was instructed in rating the pain sensitivity and unpleasantness using a trackball/response device and a computer projected VAS, after which the participant could rest until the subsequent stimulus was delivered. The time course of each heat run followed the same pattern starting with a 20 second initiating resting period followed by seven stimulus and rating/resting periods of 2 second increasing ramp stimulus, 10 second plateau stimulus, 3 second decreasing ramp stimulus and 37-38 second rating/resting.

[1] FiXme Note: ADD NAME AND BRAND

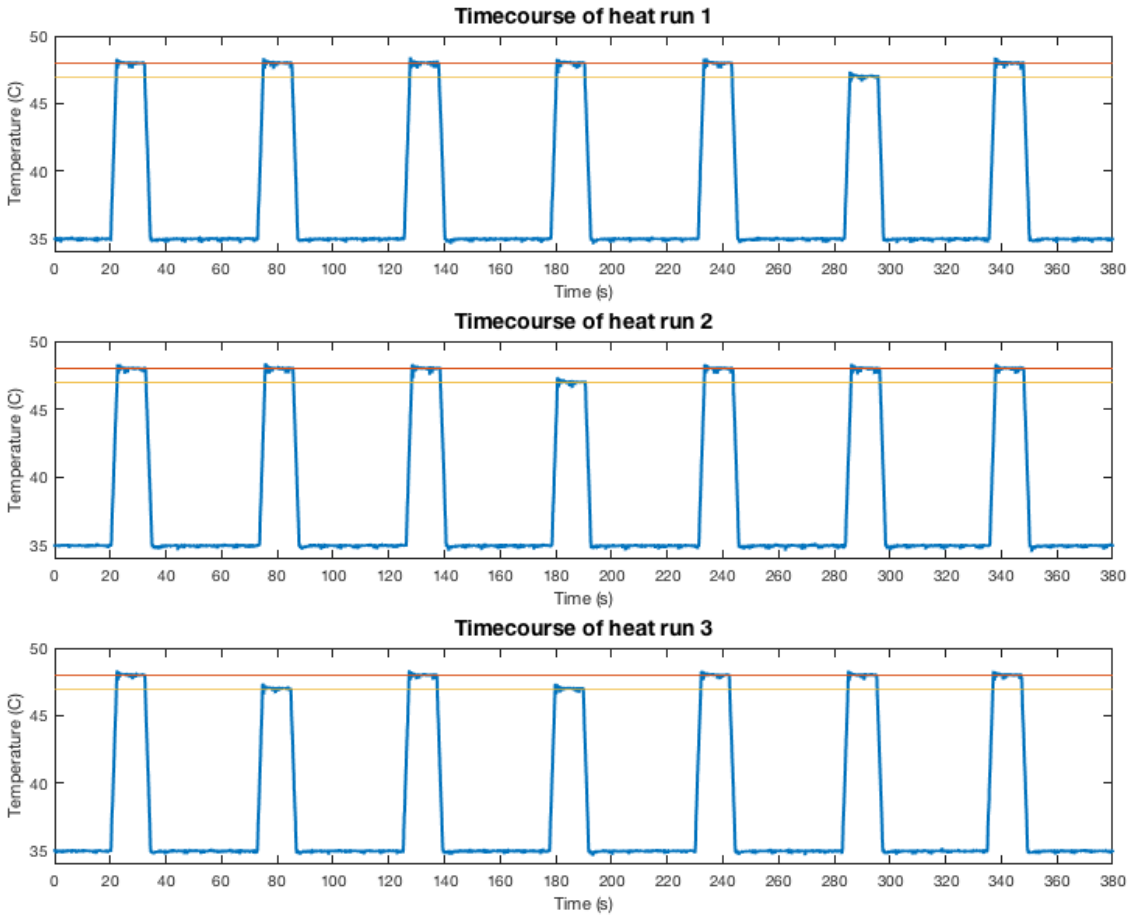

Figure 4.2: Illustrations of the time courses of heat stimuli for all three heat runs. The blue graphs depicts the temperature of the heat stimuli and the yellow and red lines are used to distinguish between 47 and 48°C. In the first heat run the 47°C stimulus was delivered during the 6th stimulus, in the second during the 4th stimulus and in the third during the 2nd and 4th stimuli. The remaining stimuli were of 48°C.

To minimize bias all participants received the same stimuli in a single-blind fashion. Furthermore, the stimuli was induced in a pseudo-random order to confine the effects of habituation and expectation.

4.2 Brain Extraction and Registration

In order to study the activation in the brain, it first has to be segmented and extracted from the surrounding tissue. To achieve an image only containing the brain, there were made use of the Brain Extraction Tool (BET), which is included in the FSL software package. As this is a standard applied method and not essential for the scope of this project, no further documentation of this step will be presented. For further documentation of BET specifications see Smith et al. [42]. BET was used for extracting the brain in both the structural T_1-weighted image and in the functional T_2^*-weighted image sequence.

The next step of preparing the functional images for analysis is to obtain the same coordinate system for these and the structural images. This step is called registration, and is done to find out more about the origin of the activation, in the form of spatial localization. As the functional images contain very low resolution activation can hardly be assessed and therefore activation can be studied by comparing the functional with a structural. This can either be achieved by registering the functional to the structural of the subject or to a standard template. The standard is made from an average of hundreds of brain. The template is useful as the spatial localization can be interpreted and reported objectively and consistently across studies. [43]
For registration in this project, first, a registration of functional to structural has been made. This was achieved by using the FSL software tool FLIRT, which uses non linear transformations. Afterwards a registration from structural to the MNI template has been made. This process utilized both non linear and linear transformations by using the FLIRT and FNIRT tool in the FSL toolbox. [44, 45]

4.3 Standard Preprocessing

Following the MRI data acquisition there are several steps, which need to be taken, before the multidimensional images are ready to undergo statistical analysis. These steps involves correction methods, which are often referred to as preprocessing. There are multiple steps in preprocessing fMR images depending on the apparent application and outcome intended. However, there is a standard set of methods that is usually used across all applications. [55] The standard basic approach to preprocessing of task-related fMRI that defines a baseline for noise removal will in the following section be described. The steps that goes in to the standard preprocessing pipeline can vary depending on the defined study design. [2]. In this project the standard preprocessing steps include: motion correction, slice timing correction, BET(Distortion correction??), spatial smoothing and temporal filtering. Figure 4.3 provides a chronological overview over the implemented steps in the standard preprocessing pipeline.

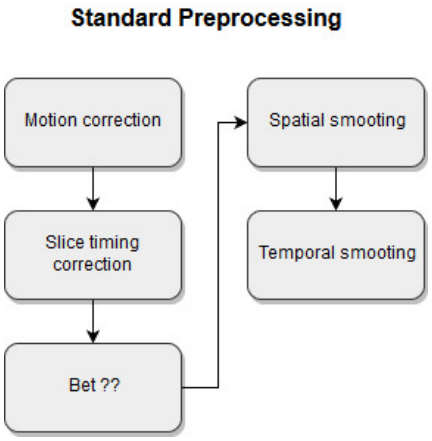

Figure 4.3: Flowchart illustrating the steps in the standard preprocessing pipeline.

[2] FiXme Note: find citation

4.3.1 Motion correction

Correcting for motion artifacts when working with fMRI is nearly inevitable, since even the best subjects will not be able to hold still during acquisition. Even subtle movements as swallowing will be visible in the acquired image. [19] To correct for these movement induced artifacts, a realignment of all volumes within a scan has been carried out using the FSL software program FMRIB's Motion Correction Linear Image Registration Tool (MCFLIRT). [**Jenkinson2002**] The tool was used to realign the series of images to a template image. The volume acquired halfway through the scan was used a reference image. This choice of template image is often justified by the middle volume being the closets to the average as well as the scanner at that time would have achieved maximum stability, as the magnetization would have reached steady state. [19] A 6 degree of freedom transformation was used to realign the images, and can therefore only correct for bulk motion. [**Jenkinson2002**]

4.3.2 Slice timing correction

When acquiring fMRI scans the slices in each volume are taken one by one. This can either be in an ascending, descending or interleaved order. Interleaved order is sequentially skipping every either odd or even slice and then afterwards acquiring the skipped slices. Ascending and descending is either from top to bottom or the opposite. Regardless of which order the slices were acquired, a misrepresentation of the hemodynamic response in each slice to the same hemodynamic response will be present due to the time difference in the slices. A representation of this effect can be seen in figure 4.4. The difference in timing for each slice constitutes a problem when analyzing the data. The data is formed into statistical model, but since this model assumes that all slices are acquired at the same time point, the actual signal and the estimated in the statistical model creates a mismatch. [19]

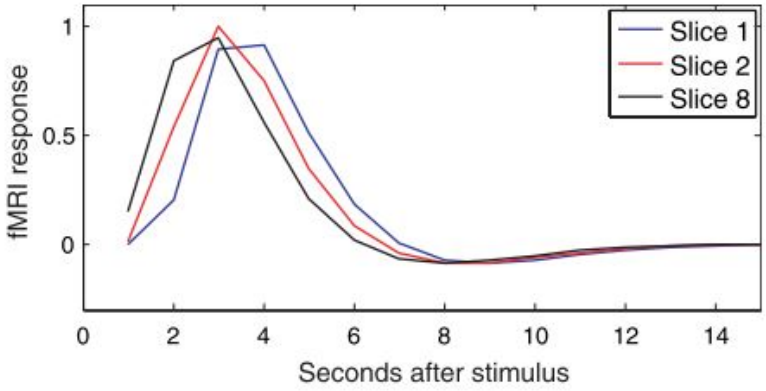

Figure 4.4: An illustration of the slice-wise acquisition effects the representation of the hemodynamic response. The response will seem to appear earlier in slice one compared to the others, as it is always the first acquired throughout the scan. [19]

To account for the mismatch in the acquisition time of each slice, a correction has been implemented using FSL software [**FMRIB2018**]. This is done by supplying the algorithm with acquisition order and the TR period. Hence, regular up and 2 second were inputed. The slice timing works by shifting the time series for the hemodynamic response curve for each slice in time to fit the middle of the TR period. This is achieved using Hanning windowed sinc interpolation. Choosing the middle slice as the reference, introduces the less interpolation, and is therefore seen as the most accurate method. [19] Hence, the slice timing correction is carried out for each of the 193 volumes in a scan.

4.3.3 Brain extraction

This step is the brain extraction of the brain in the functional scan. The extraction of the functional brain is done in the same way as presented in section 4.2.

4.3.4 Spatial smoothing

The next step in the standard preprocessing approach was to introduce spatial smoothing. Some of the image pixels will likely be contaminated with scattered noise presented higher pixel intensities. These can be removed by averaging the misrepresented pixel with its surrounding neighbors. Hence, this allows for the possibility of gaining a higher signal to noise ratio though with the consequence of a decrease in spatial resolution as the image gets blurred and smaller areas of activation gets smeared together. The operation can be justified by the closely neighboring voxel being correlated in effect to the hemodynamic response. Thereby some of the higher-frequency information removed by spatial smoothing. Furthermore spatial smoothing has the advantage that is reduces reduces the difference between subjects improving the between subject comparison. [19]
The implementation of spatial smoothing on the data was done using the Smoothing over Univalue Segment Assimilating Nucleus (SUSAN) noise reduction filter in the FSL toolbox. The 3 dimensional spatial smoothing was carried out on each volume of the FMRI data set separately. Thereby reducing noise without reducing valid activation, which should be achieved using a mask size of 5 mm full width half maximum (FWHM), thus resulting in a trade off of smoothing bigger and smaller areas of activation. An advantage of the SUSAN algorithm is its ability to distinguish between tissue types as e.g. grey matter and white matter and thereby only including intensity value from neighboring voxels which consist of the same tissue type as the voxel being smoothened. Thereby all structures in the image should be preserved. [**Smith1997**]

4.3.5 Temporal smoothing

A characteristic noise which represents itself during fMRI data is the presence of a low-frequency drift. The drift is characterized as a slow increasing trend in the BOLD magnitude, when assessing the signal in the time domain. Doing a Fourier Transform, to analyze the signal in the power spectrum, would reveal low frequency contributers influencing the

signal. As mentioned in section 4.1, the frequency of noise was 0 Hz to 0.015 Hz and the frequency band of activation is 0.01 Hz to 0.02 Hz. To dampen some of the low-frequency artifactual content a high pass filter with a cutoff frequency of 100 seconds (0.01 Hz) was implemented. [**FMRIB2018**].

4.4 FSL FIX

Top saying something about why this methods needs to be tried. The automated de-noising system FSL FIX (FMRIB's ICA-based X-noisefier), made by the Oxford university center for Functional MRI of the brain (FMRIB), provides newly proposed data driven method for de-noising fMRI scans. The method applies the use of Independent Component Analysis (ICA) and numerous classifiers, which will be explained throughout this section. [27]

4.4.1 Setting the number of ICs

After having undergone the initial standard preprocessing presented in section **??**, the next step was to extract the independent components (IC) using MELODIC. But before the data could be subjected to the ICA, several considerations were made in order to increase ICA performance. The separation of sources is highly dependent on the number of ICs (N-ICs) chosen and therefore crucial for the FIX end performance. Consequently an investigation of the optimal number of components was conducted. The risk of underestimating the number of components, would result in a loss of information and suboptimal signal extraction [46]. Contrary, overestimating the number of components would result in a false representation, as the different informative sources would be split leaving fractional sources, which would be very hard to identify and utilize [46, 47].
Data used for investigating the optimal number of components was derived from ten randomly chosen subjects having three heat runs each. This made for 30 IC analyses each completed utilizing the MELODIC tool.

Default mode

Initially no limit was selected and the MELODIC algorithm per default estimated the optimal number of components, as recommended by the MELODIC developers. [40] The MELODIC tool provided analyses with the estimated number of component to represent the variance ranging from 9-64 components. Due to the substantial amount of variability in the number of components estimated, the degree to how much the sources had been separated varied substantially between the components. Inspecting the output from the ICA, which produced nine components, it became clear that the separation of sources was not sufficient, as the components was mixtures of multiple sources of noise and signal. Furthermore no task related activation where seen in any of the components indicating that variance of noise accounted for the first nine components. Inspecting the analyses with the highest number of components, it became evident that the algorithm had over-

estimated the number of ICs, leaving empty and fractured activation in the components unrecognizable for labeling. Because of the MELODIC ICA on default mode overestimating and underestimating the number of components, a case specific analysis for the optimal number of components was conducted.

N-IC analysis

Seeking guidelines in the literature, various articles have worked with estimating the optimal number of components. In the case of Majeed et al. [48], results indicate that a N-IC lower than 5 components would lead to an underestimation and more than 50 components would result in overestimation. The optimal N-IC was found to be 10. Another study limited the number of components to 20 as this was found to preserve much of the information without overestimating [49] Furthermore other studies limited the number to 25 components [50, 51]. Building on this knowledge, MELODIC was run on the ten subjects again limiting the N-ICs to 15, 20, 25, 30 to assess which would give the optimal separation between signal and noise, and in separating the independent sources for each. The assessment was made by counting the following outcomes:

- The number of components containing signal activation from multiple sources or unrecognizable due to fragmentation.
- The number of components containing signal activation from a single source
- The number of components containing no activation

Examples of spatial maps containing multiple sources, fragmented sources and a single source can be seen in figure 4.5, figure 4.6 and figure 4.7, respectively. Identification of sources was supported by utilizing the guidelines presented in [41], showing how the different noise sources would be present in the spatial map and using the information of which brain regions would be activated during pain stimuli as presented in section 2.2. Both investigators conducted the assessment. One found 25 components to be optimal, whilst the other found that 30 components was more favorable. The assessment was assisted by incorporating consulting from an expert on the area. With help from experts advice, 25 components was identified to provide the best separation of sources in the data. This decision was well supported by the results of the prior studies of [50, 51].

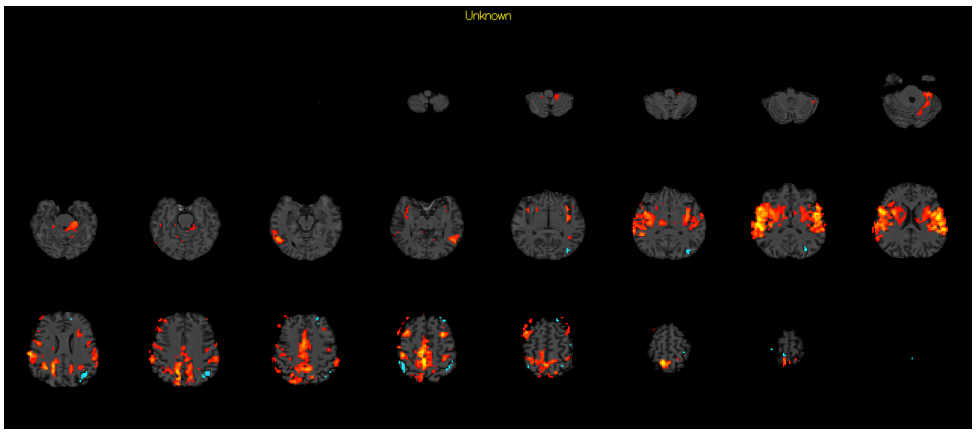

Figure 4.5: An example of a component with a spatial map for a component showing activation from multiple sources. Activation cannot be localized to single brain regions.

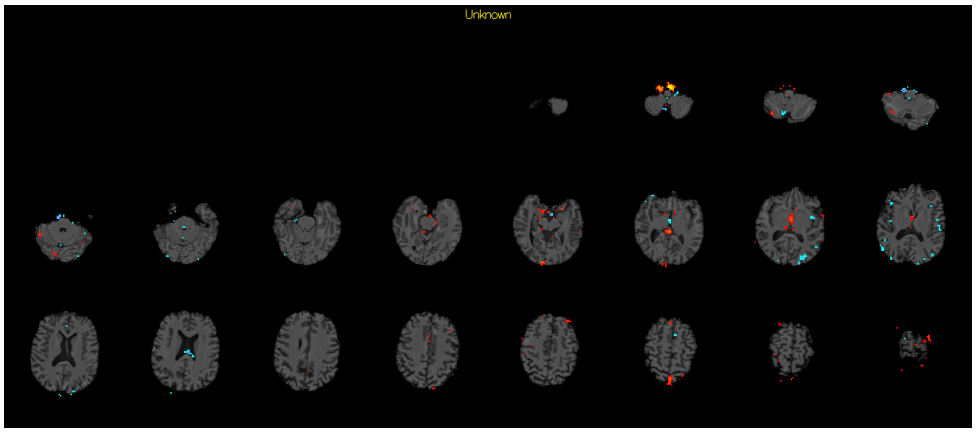

Figure 4.6: An example of a component with a fragmented spatial map illustrating that no brain activation or artifactual noise can localized.

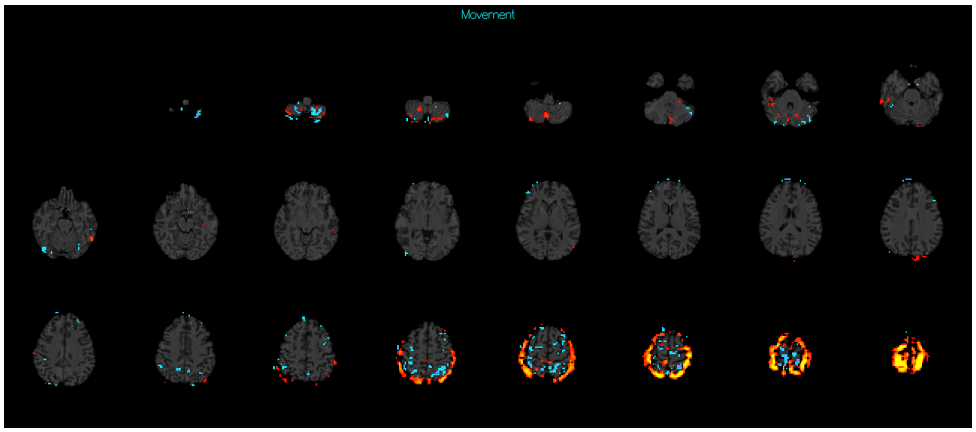

Figure 4.7: An example of a spatial map showing a clearly recognizable artifact in the form of movement dominating the component.

4.5 Hand Labeling of Independent Components

Before the automatic FIX classifier could be used to identity components of noise and interest it needed to be trained with hand labeled components [27]. For this purpose 25 components were extracted from all heat runs for 34 participants using the MELODIC program, after which each component was manually hand labeled.
The process of the hand labeling followed that the investigators labeled half of the components each, where after the labeled components were cross-checked and discussed by the investigators. The investigator assessment relied heavily on information with regards to hand labeling provided by Griffanti et al. [41] and Salimi-Khorshidi et al. [27]. As a final assessment an expert did a control and corrected labels if they not did not fit the expert opinion.
The MELODIC program proposed a set of predefined classes to label the components. The classes suited for artifacts were movement, susceptibility-motion, MRI, cardiac, respiratory, white matter, sagittal sinus and unclassified noise. One component could contain more than one artefact class. If all artefact classes of the component were identifiable, more classes were added to the component. The unclassified noise class was proposed for components containing a mixture of different artifact sources, which were less clear to pinpoint. A class named unknown was intended for labeling components that contained both noise and signal. For any signal of interest the signal class was proposed, as there was no discrimination between different types of signal of interest. The following illustrations show transverse spatial examples of components related to the various artifact classes, the signal class and the unknown class. It should be noted that the coronal and sagittal views were additionally available, along with the time course and frequency content of the components for shaping the assessment of the labeling. The corresponding structural images were used to underlay the components to assess in which brain regions the components were located.

4.6 Feature extraction

An important step in establishing a robust classification model is extracting effective features to feed the classifier. Extraction of reasonably independent features that correlate with the targeted class will establish a more robust classifier when training it. In the FIX algorithm 186 features with temporal or spatial characteristics are extracted. The first feature extracted is, however, considered of spatial-temporal origin and consists of the number of IC computed by MELODIC. It will be expected that the noise present in the data will affect the number of ICs extracted. [27] However, in this study the number of IC calculated for each heat run was fixed on 25, and that feature would therefore have no influence on the expectation of a component containing noise or signal. The following sections aim to explain the idea behind extracting these exact temporal and spatial features and to give examples of selected features. Thus, not all 186 features will be covered in depth. For a further explanation of the features we refer the reader to the 2014 study by Salimi-Khorshidi et al. [27] The result of the feature extraction for one from one heat run from one subject consisted of a 25 x 186 matrix - one feature value for

each feature of each component.

4.6.1 Temporal features

Autoregressive models Temporal features extracted were based on autoregressive (AR) properties of the time course. It was expected that the temporal smoothness derived from AR models, could help distinguish signal from particular artefact components. For an AR(n) model, where the n is the order up to $n = 6$, and a_k denotes the AR parameters. Let e_p denote the variance of the residual of up to AR(6). The first AR property features derived are the slope and intercept of the straight line which is explaining e_p as a function of n, where an increase in n will output a better fit and thus a smaller residual variance. It is expected that an improvement in goodness of fit will decrease as more noise is present in the time course. The other AR features extracted are simply a_1, a_2, e_1 and e_2. These features encapsulate the autocorrelation estimated from the low order AR models. It was expected that components containing signal would have a higher temporal autocorrelation and lower residual variance compared to components containing unstructured noise.
Distribution information It is expected that signal components would be normally distributed, while noise components would vary in how they are distributed (e.g. long-tailed distribution and multi-modal), e.g. due to sudden spikes in the time course caused by rapid movements and/or scanner artefacts. Features that give information on distribution were therefore extracted, and these include kurtosis, skewness, mean-median difference, entropy and negentropy.
Jump amplitudes The extent of jumps in the amplitude of the time course is an important feature in distinguishing signal from noise. Signal components are expected to be fairly smooth, while noise components usually will contain large jump and fluctuations. To describe this characteristic features based on division calculations that include the standard deviation (std), mean or maximum of the differential of the time course and the std, mean or maximum of the time course were extracted.
Fourier transform Taking the fast Fourier transform (fft) of the time course will capture the frequency content, which can be utilized to differentiate between signal and noise. It is expected for signal components to almost exclusively have high power amplitude in low frequencies due to the block design of the stimuli task. Noise components may on the other hand contain frequency in the whole spectrum. Therefore several fft-based features were extracted. Examples of features derived were the total power above 0.1, 0.15, 0.2 and 0.25 Hz respectively and the percentage of power that lied in the following intervals: 0:0.01, 0.01:0.025, 0.025:0.05, 0.05:0.1, 0.1:0.15, 0.15:0.2 and 0.2:0.25 Hz.
Correlation It is expected that time courses of signal components are strongly associated with grey matter (GM), while noise components will correlate with time courses of white matter (WM) and cerebrospinal fluid (CSF) along with the motion correction time courses calculated in the initial pre-processing. The last temporal features extracted were therefore based on correlation between the component time course and reference GM-, WM-, CSF-derived time courses and the motion correction time courses. The reference time courses were calculated using FSL's tissue segmentation tool, from which GM, WM and CSF masks were extracted. Each type of tissue's time course was then computed as

the average of the time courses that correspond to that given tissue. [27]

4.6.2 Spatial features

Clusters' size and spatial distribution The distribution of activated and deactivated cluster sizes is an important indicator of a component containing either noise or signal. It is expected that signal components contain small number of relatively large clusters, while noise components contain a large number of small clusters. To capture this information, a list of a spatial map's clusters, $\mathbf{c}$ was formed, where only cluster of at least 5 connected voxels are kept, and listed in descending order. Feature extracted to summarize $\mathbf{c}$ are: length($\mathbf{c}$), mean($\mathbf{c}$), median($\mathbf{c}$), max($\mathbf{c}$), var($\mathbf{c}$), skewness($\mathbf{c}$), kurtosis($\mathbf{c}$), $\mathbf{c}$[1], $\mathbf{c}$[2], and $\mathbf{c}$[3], where the last three features were the first to third elements of $\mathbf{c}$. Looking at the distribution of clusters in individual slices can help detect scanner artefacts. Let $\mathbf{V}$ and $\mathbf{U}$ contain slice specific information of the ICA spatial map $\mathbf{m}$ and slice specific information of voxels above 2.5 z-score $\mathbf{m}_\mathbf{p}^\tau$, respectively. Further features consist of max($\mathbf{V}$) and max($\mathbf{u}$) and slices containing above 15 It is not very likely for signal components to have large contents of both activation and deactivation in the spatial map. For this reason features that use the mean, standard deviation and entropy of $\mathbf{m}$ to measure the amount of positive and negative voxels in the components were extracted.
Voxels overlaying dark/bright raw data voxels As mentioned signal of interest is associated with dark voxels where noise is usually found in bright voxels. The next features are based on multiplying and dividing the components' spatial map with the mean of the corresponding pre-processed time courses, forming two new images. It is expected that the intensity information contains information on which voxels are of interest and which are not. The features consists of the 95th and 99th percentile of the new images.
Percent on brain boundary High Activation/deactivation in the spatial map that overlaps the boundary of the brain and the area outside the brain will most likely be movement related. Segmenting the brain using the FSL BET tool and subtracting this mask with and eroded version of itself will output a mask of the brain's edge. Five masks with varying thickness are extracted. The features measure how large a percentage of the components spatial maps that is imbedded in the edges and how large a percentage of edges is covered by the component. The higher these values are, the higher probability the component was to have captured a movement artefact.
Mask-based features It might be needed to use spatially-specific masks to detect certain noise sources (Sagital sinus, CSF and WM) more precisely. The spatial appearance of the major veins could for instance be mistaken for signal of interest and the cluster-like activation pattern may look similar to signal of interest. To detect these structures more conservatively FIX utilizes three standard-space masks that consist of three major veins. From the three masks three different masks with varying thickness are derived, due to the anatomical variability between subjects. The same features as in the brain boundary features are extracted, where these new masks were utilized instead. The same procedure was executed for GM.
Other spatial features Other features detect spatial smoothness. Signal components are expected to have high spatial smoothness, meaning a fairly small amount of connected

clusters, where noise components are expected to have a more patchy spatial map. Features that extract spatial smoothness in mm and voxels counts are therefore included. The last spatial features detect striped patterns of interleaved positive and negative activation. A largely striped pattern in the spatial map could imply that a component contains noise. [27]

Part III

Synthesis

Bibliography

[1] James Dahlhamer et al. “Prevalence of Chronic Pain and High-Impact Chronic Pain Among Adults - United States, 2016.” In: *MMWR. Morbidity and mortality weekly report* 67.36 (2018), pp. 1001–1006.

[2] National Center for Health Statistics Health. “Health, United States, 2006 With Chartbook on Trends in the Health of Americans”. In: (2006), p. 559.

[3] Institute of Medicine. *Relieving Pain in America: a Blueprint for Transforming Prevention, Care, Education, and Research*. Vol. 26. 2. 2011, pp. 197–198.

[4] Karen D. Davis et al. “Brain imaging tests for chronic pain: Medical, legal and ethical issues and recommendations”. In: *Nature Reviews Neurology* 13.10 (2017), pp. 624–638.

[5] Harold Merskey and Nikolai Bogduk. “Classification of Cronic Pain”. In: *International Associasion for the Study of Pain* 2 (1994).

[6] Peter Brook, Tony Pickering, and Jayne Connell. *Oxford Handbook of Pain Management*. 1st. Oxford University Press, 2011, p. 463.

[7] Eric L Garland and D Ph. “Pain Processing in the Human Nervous System: A Selective Review of Nociceptive and Biobehavioral Pathways Eric”. In: *Vickrey BG, Shekelle P, Morton S, et al. Prevention and Management of Urinary Tract Infections in Paralyzed Persons: Summary. 1999 Jan. In: AHRQ Evidence Report Summaries. Rockville (MD): Agency for Healthcare Research and Quality (US); 1998-2005. 6. Avai* 39.3 (2013), pp. 561–571.

[8] Robert F. Schmidt. *Fundamentals of Sensory Physiology*. Third edit. 1986.

[9] Christopher S. Nielsen et al. “Individual differences in pain sensitivity: Genetic and environmental contributions”. In: *Pain* 136.1-2 (2008), pp. 21–29.

[10] Robert C. Coghill. “Individual Differences in the Subjective Experience of Pain: New Insights into Mechanisms and Models”. In: 50.9 (2011), pp. 1531–1535.

[11] A Feizerfan. “Transitions from acute to chronic pain”. In: *Acute Pain Management* 15.2 (2015), pp. 98–102.

[12] Kai McGreevy, Michael M. Bottros, and Srinivasa N. Raja. “Preventing Chronic Pain following Acute Pain: Risk Factors, Preventive Strategies, and their Efficacy”. In: *European Journal of Pain Supplem* 5.2 (2011), pp. 365–372.

[13] Robert C Coghill, John G Mchaffie, and Y Yen. “Neural correlates of interindividual differences in the subjective experience of pain”. In: *Proceedings of the National Academy of Sciences* 114.48 (2003), E10507–E10507.

[14] Hyungsuk Kim et al. “Genetic influence on variability in human acute experimental pain sensitivity associated with gender, ethnicity and psychological temperament”. In: *Pain* 109.3 (2004), pp. 488–496.

[15] Nichole M. Emerson et al. “Pain Sensitivity is Inversely Related to Regional Grey Matter Density in the Brain Nichole”. In: 155.3 (2014), pp. 566–573.

[16] Irene Tracey and Patrick W. Mantyh. “The Cerebral Signature for Pain Perception and Its Modulation”. In: *Neuron* 55.3 (2007), pp. 377–391.

[17] Allan I. Basbaum et al. “Cellular and Molecular Mechanisms of Pain”. In: 139.2 (2009), pp. 1–6.

[18] Gary H Glover. “Overview of functional magnetic resonance imaging”. In: *Neurosurg Clin N Am* 22.2 (2011), pp. 133–139.

[19] Thomas Poldrack A, Russell; Mumford A, Jeanette; Nichols E. *Handbook of functional MRI data analysis*. 2011.

[20] Mushabbar A. Syed, Subha V. Ramen, and Orlando P. Simonetti. *Basic Principles of Cardiovascular MRI*. 2015, pp. 1–338.

[21] Nishanth Khanna et al. “Functional neuroimaging: fundamental principles and clinical applications”. In: *Neuroradiology Journal* 28.2 (2015), pp. 87–96.

[22] Sang Pil Lee, Afonso C. Silva, and Seong Gi Kim. “Comparison of diffusion-weighted high-resolution CBF and spin-echo BOLD fMRI at 9.4 T”. In: *Magnetic Resonance in Medicine* 47.4 (2002), pp. 736–741.

[23] J Dubois and R Adolphs. “Building a science of individual differences from fMRI”. In: *Trends in Cognitive Sciences* (2016), pp. 425–443.

[24] Robert C. Coghill et al. “Pain Intensity Processing Within the Human Brain: A Bilateral, Distributed Mechanism”. In: *Journal of Neurophysiology* 82.4 (1999), pp. 1934–1943.

[25] R Wood et al. “1.5 Tesla magnetic resonance imaging scanners compared with 3.0 Tesla magnetic resonance imaging scanners: systematic review of clinical effectiveness”. In: *CADTH Technology Overviews* 2.2 (2012), e2201.

[26] Katherine S. Button, John P. A. Ioannidis, and Claire Kokrysz. “Power failure: why small sample size undermines the reliability of neuroscience Katherine”. In: *Nature Reviews Neuroscience* 33.1 (2013), pp. 365–376.

[27] Gholamreza Salimi-Khorshidi et al. “Automatic denoising of functional MRI data: Combining independent component analysis and hierarchical fusion of classifiers”. In: *NeuroImage* 90 (2014), pp. 449–468.

[28] Kevin Murphy, Rasmus M. Birn, and Peter A. Bandettini. “Resting state fMRI confounds and cleanup”. In: *NeuroImage* 80 (2013), pp. 349–359.

[29] Chia Shang J Liu et al. “Spatial and temporal characteristics of physiological noise in fMRI at 3T”. In: *Academic Radiology* 13.3 (2006), pp. 313–323.

[30] Armin Iraji et al. “The connectivity domain: Analyzing resting state fMRI data using feature-based data-driven and model-based methods”. In: (2016), pp. 494–507.

[31] Martin Monti. “Statistical Analysis of fMRI Time-Series: A Critical Review of the GLM Approach”. In: *Frontiers in Human Neuroscience* 5.March (2011), pp. 1–13.

[32] Gary H. Glover, Tie Qiang Li, and David Ress. “Image-based method for retrospective correction of physiological motion effects in fMRI: RETROICOR”. In: *Magnetic Resonance in Medicine* 44.1 (2000), pp. 162–167.

[33] Yashar Behzadi et al. “A Component Based Noise Correction Method (CompCor) for BOLD and Perfusion Based fMRI”. In: 6.8 (2013), pp. 90–101.

[34] Martin J Mckeown et al. “Analysis of fMRI Data by Blind Separation Into Independent Spatial Components”. In: 188.June 1997 (1998), pp. 160–188.

[35] V. D. Calhoun et al. “fMRI activation in a visual-perception task: Network of areas detected using the general linear model and independent components analysis”. In: *NeuroImage* 14.5 (2001), pp. 1080–1088.

[36] Johnathan Deslauriers et al. “Increase of posterior connectivity in aging within the Ventral Attention Network: A functional connectivity analysis using independent component analysis”. In: *Brain Research* 1657 (2017), pp. 288–296.

[37] Linden Parkes et al. “An evaluation of the efficacy, reliability, and sensitivity of motion correction strategies for resting-state functional MRI”. In: *NeuroImage* 171.July 2017 (2018), pp. 415–436.

[38] Yuhui Du et al. “Identifying functional network changing patterns in individuals at clinical high-risk for psychosis and patients with early illness schizophrenia: A group ICA study”. In: *NeuroImage: Clinical* 17.May (2018), pp. 335–346.

[39] Jussi Tohka et al. “Automatic independent component labeling for artifact removal in fMRI”. In: *NeuroImage* 39.3 (2008), pp. 1227–1245.

[40] Oxford Centre for Functional Magnetic Resonance and Imaging of the Brain (FMRIB); *MELODIC/FAQ*. 2016.

[41] Ludovica Griffanti et al. “Hand classification of fMRI ICA noise components”. In: *NeuroImage* 154.June 2016 (2017), pp. 188–205.

[42] Stephen M. Smith. “Fast robust automated brain extraction”. In: *Human Brain Mapping* 17.3 (2002), pp. 143–155.

[43] Joseph V. Hajnal, Derek L.G. Hill, and David J. Hawkes. *Medical Image Registration*. Mecheal R. Vol. 39. 5. The BIOMEDICAL ENGINEERING Series, 2001, p. 394.

[44] JLR Andersson, M Jenkinson, and S Smith. “Non-linear registration aka Spatial normalization. FMRIB Tech Rep TR07JA2.” In: June (2007).

[45] Mark Jenkinson and Stephen Smith. “A global optimisation method for robust affine registration of brain images”. In: *Medical Image Analysis* 5.2 (2001), pp. 143–156.

[46] Christian F. Beckmann and Stephen M. Smith. “Probabilistic Independent Component Analysis for Functional Magnetic Resonance Imaging”. In: *IEEE Transactions on Medical Imaging* 23.2 (2004), pp. 137–152.

[47] Yi-Ou Li, Tülay Adalı, and Vince D. Calhoun. "Estimating the number of independent components for functional magnetic resonance imaging data". In: *Human Brain Mapping* 28.11 (2007), pp. 1251–1266.

[48] Waqas Majeed and Malcolm J. Avison. "Robust data driven model order estimation for independent component analysis of fMRI data with low contrast to noise". In: *PLoS ONE* 9.4 (2014).

[49] V.D. Calhoun et al. "Spatial and temporal independent component analysis of functional MRI data containing a pair of task-related waveforms". In: *Human Brain Mapping* 13.1 (2001), pp. 43–53.

[50] Jieun Kim et al. "Sustained deep-tissue pain alters functional brain connectivity". In: *Pain* 154.8 (2013), pp. 1343–1351.

[51] Nathalie Erpelding and Karen D. Davis. "Neural underpinnings of behavioural strategies that prioritize either cognitive task performance or pain". In: *Pain* 154.10 (2013), pp. 2060–2071.

[52] A. A. Bharath. *Introductory Medical Imaging*. Vol. 3. 1. 2008, pp. 1–186.

[53] John C Edwards. "Principles of NMR". In: ().

[54] Govind B. Chavhan et al. "Principles, Techniques, and Applications of T2*-based MR Imaging and Its Special Applications". In: *RadioGraphics* 29.5 (2009), pp. 1433–1449.

[55] Massieh Moayedi, Tim V. Salomons, and Lauren Y. Atlas. "Pain Neuroimaging in Humans: A Primer for Beginners and Non-Imagers". In: *Journal of Pain* 19.9 (2018), 961.e1–961.e21.

[56] Michael W L Chee et al. "Comparison of block and event-related fMRI designs in evaluating the word-frequency effect". In: *Human Brain Mapping* 18.3 (2003), pp. 186–193.

[57] A Hyvärinen, Juha Karhunen, and Erkki Oja. "Independent Component Analysis". In: (2001).

[58] A Hyvärinen and Erkki Oja. "Independent component analysis: algorithms and applications." In: *Neural networks : the official journal of the International Neural Network Society* 13.4-5 (2000), pp. 411–30.

[59] John L Semmlow. *Biosignal and Biomedical Image Processing*. 2004.

[60] CIS 520. *PCA*. 2018.

[61] Y Murali Mohan Babu. "PCA based image denoising". In: *Signal & Image Processing : An International Journal* 3.2 (2012), pp. 236–244.

[62] Jean Baptiste Poline and Matthew Brett. "The general linear model and fMRI: Does love last forever?" In: *NeuroImage* 62.2 (2012), pp. 871–880.

A | Appendices

A.1 MRI physics

Magnetic Resonance Imaging (MRI) is a non-invasive imaging technology, which does not involve potentially damaging ionizing radiation as in other scanners, eg. CT and X-ray. MRI is especially suited for representing soft tissue portions of the body, which makes it a widely used technology in brain imaging, both for clinical and research purposes, as it can depict the anatomical structure at a millimeter resolution. This section will provide information on the physics behind MRI and which physiological properties that can be exploited to create an image of the body.

Magnetic resonance imaging (MRI) is founded on the principle of nuclear magnetic resonance (NMR), which exploits the magnetic properties of the hydrogen nucleus that contains a single proton. The proton is not static, but rotates around its own axis. As the proton is positively charged it creates a magnetic moment in the direction described by the thumb rule, and can interact with an external magnetic field. The human body consists of approximately 10% hydrogen atoms, but as the hydrogen nuclei spins are randomly orientated, the net magnetic moment equals zero, as the nuclei cancel each other out. Placing the body in a strong magnetic field will align the nuclei. A property of the hydrogen nucleus is its quantum spin rate, which can either be $\frac{1}{2}$ or $-\frac{1}{2}$ either in the direction or the opposite direction of the main magnetic field. Most will align in the direction of the magnetic field, while the rest align in the opposite direction, possibly as a result of heat radiation absorbed by the nuclei. The direction of the nucleus is determined by its energy level, leaving the former in a low energy state and the latter in a high energy state. The nuclei do not simply point in the direction or opposite the direction of the magnetic field, but precess. [52] The rate of precession can be calculated by the Lamour frequency:

$$f = y * B_0 \tag{A.1}$$

f is precession frequency, y is gyroscopic ratio and B_0 is magnetic field strength. The equation states that the precession frequency is proportional to the strength of the magnetic field. After canceling out all opposing precessing nuclei, the net magnetization, or longitudinal magnetization, will point in the direction of the external magnetic field. However, the longitudinal magnetization can not be detected directly as it points in the direction of the strong external magnetic field. Additional techniques are therefore used in NMR, to facilitate a detectable signal. [52] A depiction of how the nucleus precessing can either align along or opposite to the magnetic field depending on its energy state, can be found in figure A.1.

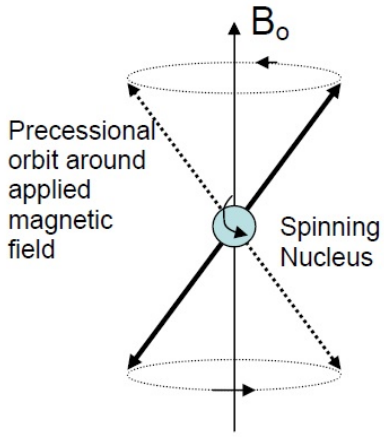

Figure A.1: The figure illustrates how the nucleus precess and spin in relation to the applied magnetic field B_0 surrounding it. The vectors, indicating the precessing, can go opposite or along the magnetic field depending on the nucleus energy state. [53]

A radio frequency pulse (RF pulse) tuned to the precession of the nuclei is transmitted in the vicinity of the nuclei. The RF pulse is absorbed by the nuclei and more, favorably half of the targeted nuclei population, will enter the high energy state, leaving the longitudinal magnetization to equal zero. The number of nuclei that flip is determined by the amount of energy the RF pulse injects, and the nuclei only exchange energy efficiently if the frequency of the energy from the RF pulse matches the precession rate. The RF pulse furthermore shifts the precession of the nuclei into same phase angle, which creates resonance, and a net magnetization pointing 90° to the longitudinal magnetization. This magnetization is called the transverse magnetization. The coherent nuclei produce a radio signal, or free induction decay signal (FID signal), that can be detected by a radio antenna. After the RF pulse is removed, the nuclei will relax into baseline state. Firstly, the spins of the nuclei will repel each other, as they are positively charged, and thus shift phase. The net magnetization will return to zero. This relaxation is called T_2 or "spin-spin" relaxation, as the energy exchange between the nucleus spins is causing the relaxation. An illustration of the T_2 relaxation can be seen in figure A.2.

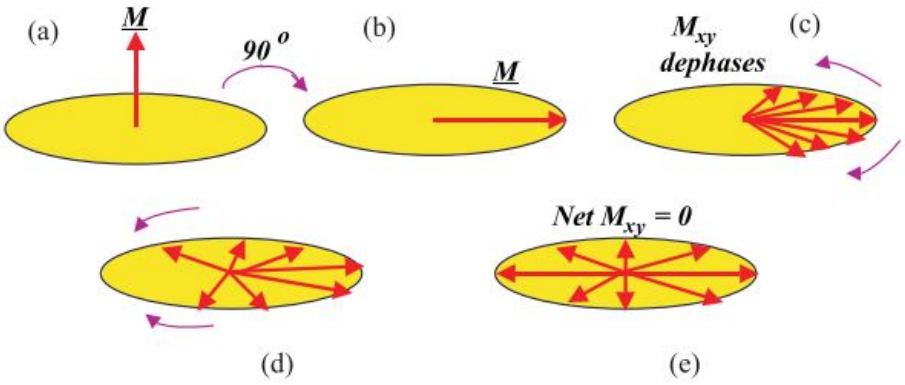

Figure A.2: An illustration of the T_2 relaxation. Before the RF pulse is emitted the majority of the nuclei are precessing out of phase in the low energy state and the net magnetization is pointing in the direction of the longitudinal magnetization, (a). The nuclei absorb the RF pulse, the magnetization shifts 90° and the nuclei precess in phase, which leaves a high transverse magnetization and FID-signal, (b). Due to interaction between the nuclei spins, the nuclei gradually dephase, until the net magnetization is 0, which is referred to as T_2 relaxation. [52]

A second relaxation appears as the high energy nuclei returns to the low energy state. The energy that was previously absorbed by the nuclei is dissipated in to the surrounding lattice in the form of heat. During this relaxation the longitudinal magnetization is regrown. This relaxation is called T_1 or "spin-lattice" relaxation, as the spins transfer energy to the surrounding lattice. [52] The hydrogen nuclei are located in different local environments in the body. Some are for instance associated with free-floating water molecules, while others are associated with structural and storage molecules such as proteins and lipids, and thus more fixed in position. The nuclei have different T_1 and T_2 relaxation characteristics, depending on the local environment or tissue they are associated with. This can be accentuated and measured in NMR. [52]
The chosen pulse sequence is key to how the tissue will be portrayed in an image, and is described by the T_{echo}, time before the FID signal is measured, and T_{rep}, time before a new RF pulse is applied. In a case of nuclei associated with lipids and water molecules, the nuclei in lipids are fixed and will have a fast T_1 relaxation after exposure to a RF pulse. Meanwhile the nuclei in the water molecules will maintain being in a synchronized phase. At T_{echo}, the nuclei associated with the lipids will have a low amplitude FID signal, as the transverse magnetization is weak, and the nuclei associated with the water molecules will have a high amplitude FID signal, as the transverse magnetization is strong. The water molecules will be assigned a white color on a greyscale image and the lipids as dark grey/black. In this case there is a long T_{echo} and a long T_{rep}, and is referred to as T_2-weighted MRI A commonly used T_2 pulse sequence is the spin echo (SE). Due to magnetic field inhomogenities the nuclei dephase more rapidly. Applying a second RF pulse of 180°after the nuclei have dephased, the nuclei will rephase. Again the constrast in the image is expressed as a result of the relaxation time of the nuclei, which is depends on the surrounding environment. . [52]
In case of T_1-weighted MRI, the T_{echo} and T_{rep} are short. As in T_2-weighted MRI a RF pulse is applied and the nuclei associated with lipids will quickly return to baseline state

and the water molecule nuclei will remain a strong transverse magnetization. At this time point a second RF pulse will be induced, referring to the short T_{rep}. Now the lipid nuclei will return to a strong transverse magnetization state and excite a high FID signal. More low energy state nuclei of the water molecules will absorb the RF pulse and shift to a high energy state, leaving a majority of nuclei in a high energy state. The water molecule nuclei now has a weak transverse magnetization and 180 degrees longitudinal magnetization, thus producing a low-amplitude FID signal. A short T_{echo} after the second RF pulse then shows lipids as white and the water molecules as dark grey/black in a greyscale image. [52]

T_2 relaxation was defined as dephasing due to energy exchange between nuclei. In practice the T_2 relaxation time happens much faster than would be predicted by these natural atomic interactions. Another factor in the dephasing of nuclei is inhomogeneities in the magnetic field. This observed T_2 relaxation is referred to as T_2^* relaxation. In a T_2^* -weighted MRI, a gradient echo (GRE) is used instead of a SE. In a GRE pulse sequence only one RF pulse is emitted with a low flip angle, and the echo time is therefore usually shorter. A gradient is applied after the initiating RF pulse, which enhances the dephasing. When the net magnetization is zero a rephasing gradient with opposite polarity of the dephasing gradient is turned on, which reverses the phase shift. A FID-signal is produced as a GRE. The gradient only reverses the phase shifts that have been affected by the gradient itself, and not those affected by magnetic field inhomogeneities. Contrast in tissues is therefore not decided through natural T_2 relaxation but by T_2^*. Thus, T_2^* -weighted MRI only works well in scanners that do not lack magnetic field homogeneity. Due to the fast acquisition time T_2^* -weighted MRI is widely used in functional MRI to image brain activity. [54]

A.2 MR image reconstruction

Different pulse sequences and certain physiological properties that can be exploited with certain pulse sequences, have been laid out in the previous sections. This section aims to describe how the corresponding echo signals are reconstructed as a MR image.

Following the Lamour frequency equation (A.1), the main magnetic field causes all hydrogen nuclei to precess with the same frequency. Without any specification of spatial localization a MRI of a human body would consist of a single number. To prevent this, separate coils in the x, y and z directions are introduced. These coils can be adjusted in position, and thus produce gradient magnetic fields with a varying strength depending on position. According to the Lamour frequency the nuclei will precess with different frequencies when in a magnetic field with varying strength. The gradients can be turned on in combination to create any direction in space. These varying frequencies can be exploited to separate parts of the anatomy and ultimately illustrate a desired area. As mentioned, the nuclei only exchange energy efficiently if the frequency of energy, or RF pulse, matches the precession rate. Thus, by altering the magnetic field along the body in one direction, z-direction for the sake of the example, the nuclei will have slightly different

precession rates, and the RF pulse will only efficiently affect a desired slice of the nuclei. The nuclei of that slice now precess at the same rate. To get an image with a spatial resolution, the voxels that make out the image needs to be discriminated between. By turning on the gradient of the x-direction the lines in the y-direction are now encoded with a particular frequency. This gradient functions as a frequency encoding gradient, and is illustrated in figure A.3. [52]

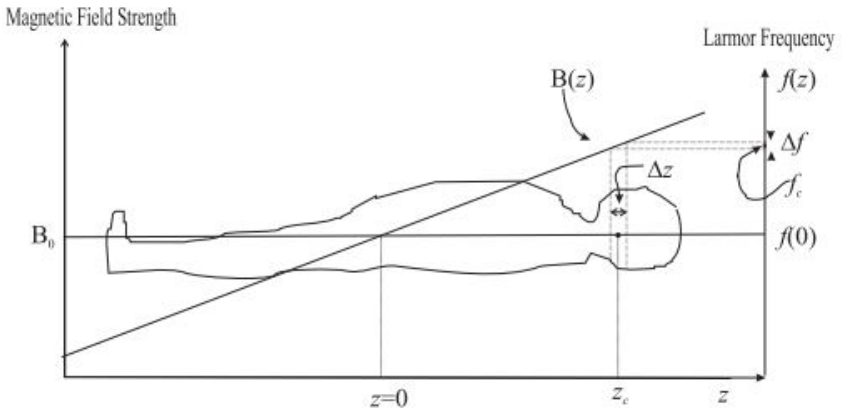

Figure A.3: The position of the slice is specified through the direction of the frequency encoding gradient ($B(z)$) and though the central frequency of the emitted RF pulse (f_c). The thickness of the slice is dependent on the steepness slope of $B(z)$, and on the bandwith of the emitted RF pulse (δf). [52]

Turning the y-gradient on and quickly off, will de-phase the nuclei while still remaining the same frequency as before. This gradient functions as a phase encoding gradient. When comparing two locations approximately one voxel apart in the x-direction, then based on the amount of gradient strength difference, there will be a certain amount of change in phase between the spins spread across that distance. The farther away from isocenter, where the magnetic field strength is B_0, the higher the change in phase will be. This notion is used to assign the correct spatial location of each voxel, when reconstructing the FID signals into an image. This phase encoding procedure is done in different gradient strengths in iterations to assign unique phases to the nuclei in the both directions. One iteration of a certain strength of the phase encoding gradient followed by a measurement is performed at a time. The only change per iteration is the phase encoding gradient strength. These iterations are then series of measurements acquired at different points in time, where each entry of the slice then represent a certain signal intensity. This time domain measurement is referred to at the raw data. [52]
The next step is to Fourier Transform (FT) the raw data, which will yield frequency information to the acquired signal intensities. This step gives a summation of the signal intensities at the different frequencies produced by the frequency encoding gradient. This is called the k-space, as the k-numbers of a signal describes its relative orientation and frequency. The k-space image contains the contrast in the center and the resolution in the periphery, as there is low or no phase encoding at the center and increasing towards the periphery, giving more brightness in the center and dimmer tones in the periphery. To

allocate the voxels in correct spatial localization an inverse 2D discrete FT is performed on the k-space image. This provides the desired image of the anatomy slice. [52] Figure A.4 shows the acquired signal in k-space and the reconstructed image after the Fourier Transform.

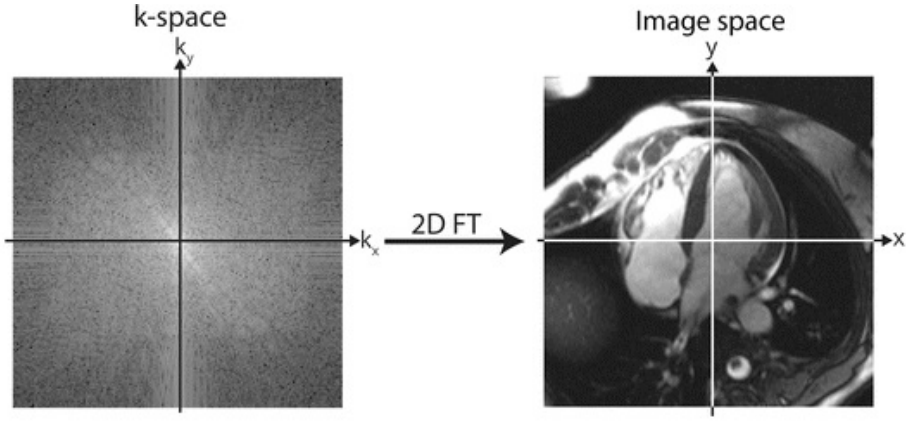

Figure A.4: A depiction of the acquired signal represented in k-space and the resulting reconstructed image after the inverse 2D Fourier Transform [20].

A.3 Stimuli Design

The following section will describe different standards of designing experiments where the impact of a given stimuli is used to assess the subsequent brain activation. The impact of stimuli on the hemodynamic response and how it is transformed into the hemodynamic response function (HRF) used analysis will be further explained, adding to the knowledge gained in section **??**.

In order to accomplish a well designed experiment, the researcher must consider the multiple types of stimuli delivered, including the form and duration of these. The researcher must be aware of the timing of events in the scanning session and any responses provoked. Additionally, the researcher should have general knowledge of where in the brain activation is seen and how the hemodynamic response will be presented. [55]

Doing cognitive experiments using fMRI, two main design types are utilized, by either using a block- or event-related design. Event-related design is inducing a series of very short lasting stimuli used to investigate single hemodynamic response. A characteristic of this method is that it permits the possibility of increasing and decreasing the interval between stimuli. Thereby the theoretical likelihood of subject confounds should be reduced as the interval would not become predictable. Event-related stimuli design further allows more temporals characteristics to be inspected, compared to a block design. Characteristics could be hemodynamic response in duration and amplitude. [56]
Block design works by performing a series of less but longer stimuli. Block designs are ideal for experiments involving detection of small differences in BOLD signal across various test

conditions where its statistical power is superior. Furthermore, if there is artifacts present they are more easily detected in the signal time course, because of the signals temporal structure. A block design is easier to design than an event-related, as randomization of intervals of stimuli is not required. The design instead focuses on the total number of stimuli used, block length, inter stimulus interval, block length and TR. An illustration of both design types can be found in figure A.5. [56]

To enable use of the hemodynamic response in fMRI analysis, it needs to be transformed in order to represent the ideal physiologic response to the stimulus. Thus, portraying the biological delay from stimuli to response. Therefore stimulus in the design is combined with the hemodynamic response function through convolution. Thus making a function that models how the BOLD signal would be represented if the voxel activity increased in a given area each time stimuli is induced. [55]

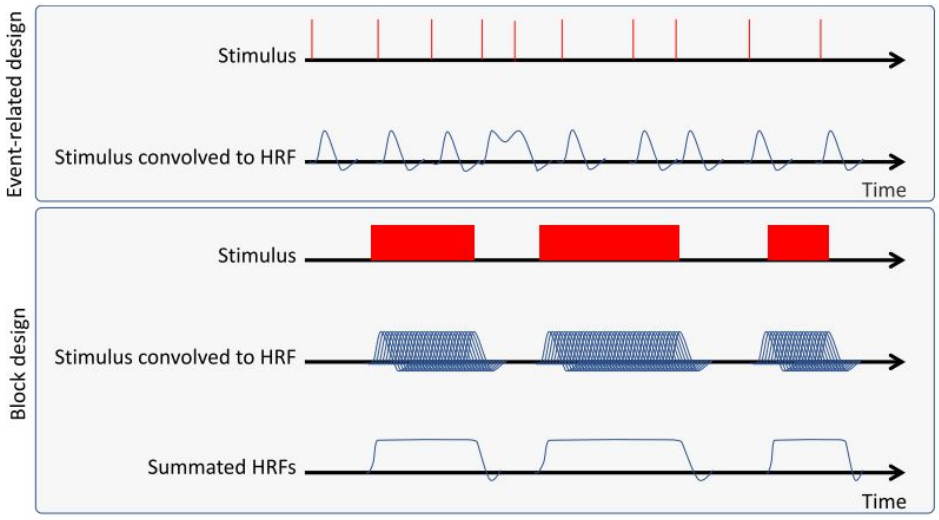

Figure A.5: The top image show the event-related stimuli design and the stimulus convolved with the hemodynamic response function. The lower image depicts a block design, the stimulus convolved with hemodynamic response function and the summated HRF response. [55]

A.4 Independent Component Analysis

Independent component analysis has proven to be a very useful tool in separating noise from wanted signal in many application. The methods has been adapted to work in BOLD-signals, making it a very desirable tool in fMRI. [27] The following section will seek to elucidate the general basic theoretical background behind the analysis exposing it possible use in this project.

The basic idea about Independent Component Analysis (ICA) is to recover m signal sources, which are mixed in n observed signals. The observed signal is given by [57]:

$$\mathbf{x} = \mathbf{A}\mathbf{s} \tag{A.2}$$

where $\mathbf{x}$ is a observed signal vector containing the mixed signal elements $x_1, x_2, ..., x_n$, $\mathbf{s}$ is the source signal vector with the elements $s_1, s_2, ..., s_m$ and $\mathbf{A}$ is a mixing matrix with the dimension $n \times m$. Note that the dimensions of the mixing matrix can be equal to each other, meaning that it is required to have at least the number of observed signals as the source signals. The observed signal is assumed to be a linear mix of independent source signals. When performing ICA the goal is to find an inverted mixing matrix A^{-1} that recovers the source signal [57]:

$$\mathbf{s} = \mathbf{A^{-1}x} \tag{A.3}$$

This can easily be achieved if the mixing matrix is known. However, this is rarely the case, as both the mixing matrix and source signals are unknown. There is no reliable way, to fully determine $\mathbf{s}$, thus a set of assumptions are required, which the ICA method is based on [57]:

- The independent components (IC)'s are assumed to be statistically independent.
- The IC's must be non-Gaussian distributions.

Regarding the assumption of independence, a set of variables $y_1, y_2, ..., y_n$ is not allowed to share mutual information so that $i \neq j$. This can be expressed as the joint probability of the variables is equal the product of each marginal probability of the variables [57]:

$$p(y_1, y_2, \ldots, y_n) = p(y_1) \cdot p(y_2) \cdot ... \cdot p(y_n) \tag{A.4}$$

Satisfying this condition assures independency of the variables. A graphical example of independence in two dimensions is shown in figure A.6 [57, 58].

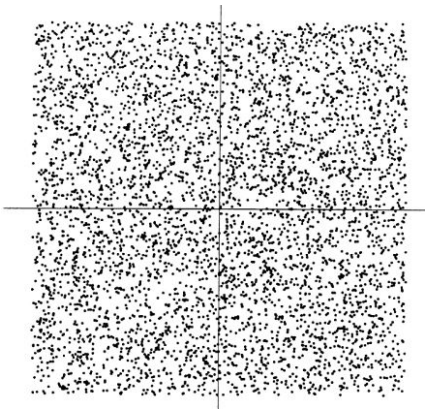

Figure A.6: Figure illustrating the joint distribution of two independent components having uniform distribution. [58].

It is clear to see that information about a variable on the horizontal axis does not give any information about variables at vertical axis and vice versa. Note that uncorrelatedness does not equal independency. However, whitening of the observed signals and thus

ensuring uncorrelatedness is very helpful in solving the ICA problem. Whitening of the data is archived by performing a linear transformation that transforms the components so that the covariance matrix equals the identity matrix, thus having unit-variance. This can be expressed through performing a linear transformation of $\mathbf{x}$ into a random vector $\mathbf{z}$:

$$\mathbf{z} = \mathbf{V}\mathbf{x} = \mathbf{V}\mathbf{A}\mathbf{s} \tag{A.5}$$

A graphical example of whitened data in two dimensions is shown in figure A.7 [57, 58].

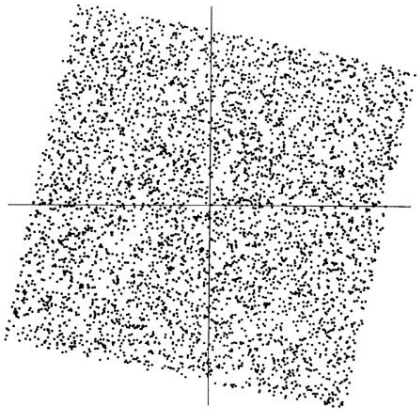

Figure A.7: Figure illustrating the impact of whitening on the joint distribution of two components [58].

The squared distribution is clearly a rotated form of the independent data. What is left to ensure independence and solving the ICA problem is to estimate an angle that gives the correct rotation. Concerning the second assumption on non-Gaussianity, the joint distribution of uncorrelated Gaussian distributions are not necessarily independent, and the distribution will be symmetrical and no information on the direction of the distribution can be derived. Thus, no transformation that allows independency can be performed, and the mixing matrix $\mathbf{A}$ can not be estimated from the mixtures. This can be shown in a two dimensional example with two sources s_1 and s_2 and the mixing matrix $\mathbf{A}$, the joint probability density function (pdf) of Gaussian distributions is calculated as [57]:

$$\begin{aligned} p(s_1, s_2) &= \frac{1}{2\pi} exp(-\frac{s_1^2 + s_2^2}{2}) \\ &= \frac{1}{2\pi} exp(-\frac{\parallel \mathbf{s} \parallel^2}{2}) \end{aligned} \tag{A.6}$$

For an orthogonal mixing matrix $\mathbf{A}$ the inverse can be written as $\mathbf{A^{-1}} = \mathbf{A^T}$, and then $\mathbf{s} = \mathbf{A^T}\mathbf{x}$. The joint pdf can then be rewritten as:

$$p(x_1, x_2) = \frac{1}{2\pi} exp(-\frac{\parallel \mathbf{A^T}\mathbf{x} \parallel^2}{2}) \mid Det(\mathbf{A^T}) \mid \tag{A.7}$$

Because $\| \mathbf{A^T x} \|^2 = \| \mathbf{x} \|^2$ and $| Det(\mathbf{A^T}) | = 1$, hence the orthogonality of $\mathbf{A}$, the joint pdf is:

$$p(x_1, x_2) = \frac{1}{2\pi} exp(-\frac{\| \mathbf{s} \|^2}{2}) \tag{A.8}$$

The joint pdf is not changed when choosing an orthogonal mixing matrix as well as the property of independence. No further information about the mixing matrix can thus be revealed when the source signals are from a Gaussian distribution. [57]

A.4.1 ICA approaches

As the mixing matrix and source signal most often are unknown, the IC's must be approximated in an iterative process. There are two main ICA iteration approaches: minimizing mutual information and maximizing non-Gaussianity. The former approach seeks to minimize mutual information by maximizing independence between components. In practice this is done by minimizing the difference between the joint density distribution and the product of the marginal density functions, the left-hand side and right-hand side of equation (A.4). This can for instance be done through a Kullback-Leibler divergence between the $p(y_1, y_2)$ and $p(y_1) * p(y_2)$ in a two dimensional case. The second approach seeks to maximize non-Gaussianity of the components. The central limit theorem states that if sources are mixed, the mix tend to get more Gaussian than the individual sources. The strategy here is to find the directions in the data that is as far away from Gaussian as possible through a linear transformation. That direction will most likely be independent components. To find these directions different ICA approaches use fourth order moments and negentropy of the data. [57]

A.5 Principal Component Analysis

The use of principal component analysis (PCA) in denoising algorithms has been exploited in various studies, showing that the properties of the PCA might be useful [33]. In this section the theory and common use of PCA is presented, including a small part on its use in images.

Principal Component Analysis (PCA) is a well renowned and widely used analysis tool, capable of finding the most defining variables in a dataset. This facilitates finding the components that are the most saying for the dataset. This introduces the possibility of dimensionality reduction by lowering the amount of redundant information. The PCA is used to transform a set possibly correlated variables into a set of uncorrelated components, called principle components. Each principal component (PC) is orthogonal on the former and are uncorrelated and have zero covariance. They each define the largest variance in an axis, such that PC 1 describes the direction of the maximum variance of the dataset. Each following PC describes the next highest variance of the dataset, with the constraint that it is orthogonal and has zero covariance with any of the former PCs. PCA is the orthogonal projection of data onto a lower dimension linear space. A PC is found by minimizing the variance by projecting the feature values (blue dots) onto the line (now

red dots) describing the highest variance in the data set (black line) as seen on figure A.8. The PC is found by minimizing the mean square distance between the data points. [59]

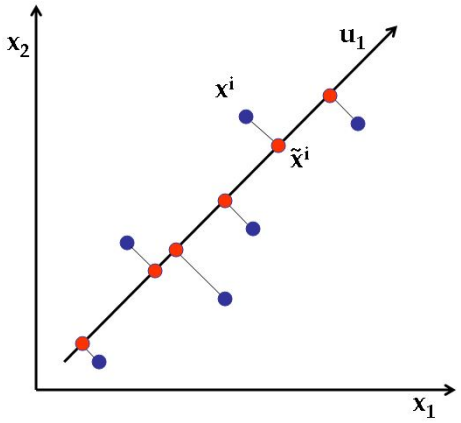

Figure A.8: Two-dimensional example of projection of data variables (blue dots) onto a PC axes (black line). (u_1) indicates the direction of the eigenvector. [60]

The algebraic method of calculating the PCs can be done by using Singular Value Decomposition (SVD). The first step is to compute the squared cross product matrix of variances and covariances among every pair of the variables in the data set, where the diagonals are the variances and the off-diagonals are the covariances, as done in the following equation:

$$S = X'X \tag{A.9}$$

Where S is the cross product and X is the dataset matrix. When finding the PCs it includes an eigen-analysis of S. The eigenvalues of are solutions to the following equation:

$$|S - \lambda I| = 0 \tag{A.10}$$

Where λ is the variances of each PC and I is the identity matrix. After solving for λ the eigenvectors can be solved through the following equation:

$$det|S - \lambda I|b_i = 0 \tag{A.11}$$

Where b_i is used to calculate the eigenvectors as in:

$$u_i = \frac{b_i}{\sqrt{b_i' b_i}} \tag{A.12}$$

Where u_i is the i number of eigenvectors that contain a contribution to the principal components. The SVD orders the eigenvalues by size $\lambda_1 > \lambda_2 \ldots > \lambda_i$. The scores for each PC is equal to the corresponding eigenvalue for that exact axis. The eigenvalues describe how much of the variance is accounted for by the associated PC. Summation of all eigenvalues accounts for the total variance of the data set; this is called the trace. To find how much the each PC accounts for, the eigenvalue of that PC is divided by the total variance: $\%\ of\ total\ variance\ = \frac{\lambda_i}{Trace}$. This can be used for deciding how many components are significant and by how much the dataset can be reduced. [59]

A.5.1 PCA in images

The PCA can also be implemented on images, where the dimensionality reduction principle is mostly used for image compression. Here images can be reconstructed using only very few principle components without much information loss. Similarly PCA can be used to de-noise images, as noise would be presented in some of the less saying components, and by removing these, noise would be removed from the image.
The PCA can be run on the entire image, but methods introducing local PCA in smaller windows of the image, have also been introduced for noise removal. [61]

A.6 General Linear Model

In order to determine if a task or stimuli has made a significant contribution to the measured BOLD signal, each voxel in the scan needs to be evaluated. The following section will therefore seek to explain a method of how to determine if any significant change is found. In this project the general linear model (GLM) will be explained and applied as it is the most used and recognized tool for fMRI analysis during the past 20 years [62].

The GLM is a well considered and used analysis tool constituting a simple way of doing standard statistical analysis on fMRI. The overall goal of the GLM model is to determine how well the time course of the scan corresponds to the known used experimental interference. In an fMRI case, that means, how well the BOLD signal over time fits the time course of the predicted signal given by the imposed stimuli, that causes brain activity. This statistical test is carried out for each voxel independently of its neighbor across the scan resulting in thousands of statistical tests in one scan. [55, 31] To explain the implementation of a GLM we can use the example presented by [31]. An acquired BOLD signal will throughout a time series, of n images, have a varying output signal. The signal in a voxel Y, at any time point, can be seen as a summation of predictor variables (regressors of interest) X and nuisance regressors (regressors of none-interest) that model noise X, a scaling parameter for each regressor β, and an error term ϵ. This can be presented in the GLM's basic from as [31]:

$$Y = X\beta + \epsilon \tag{A.13}$$

Expanding this formulation into a complete scan, including multiple regressors, can be presented on a matrix form. A depiction of a GLM design matrix incorporating the factors making up the BOLD signal can be seen in figure A.9.

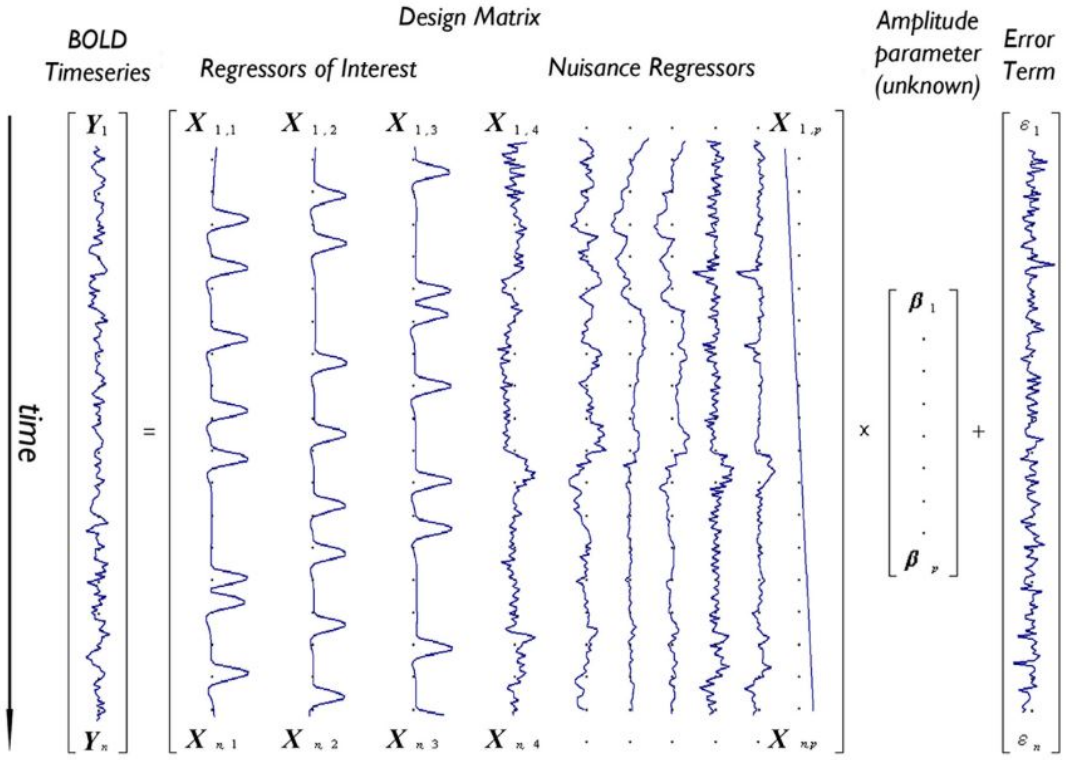

Figure A.9: Illustration of a design matrix for a given GLM model, describing the BOLD time series Y_n, the regressors of interest $X_{1,1}, X_{1,2}, X_{1,3}$, the nuisance regressors $X_{4..p}$, the amplitude parameter $\beta_{1..p}$ and the error terms $\epsilon_{1..n}$. [31]

The predictor variables are found by modeling what is known or predicted as output. The predictors of interest would come from hemodynamic response curve convoluted with stimuli design as presented in section A.3. GLM models will often introduce nuisance predictors as well used to model variables such low frequency drift and motion to make a more robust model. These are non interest regressors, as they do not resemble the wanted signal, being the stimuli induced. The amplitude parameter is the unknown weight, scaling the magnitude of resemblance between each predictor value and the output. They describe the strength of the relationship between that regressor and the voxel's BOLD signal course of activation. The error term contains the value for each observation, which can not be explained by the weighted sum of the amplitude parameter. [55, 31]

The goal is to estimate the value of the scaling parameter β for all regressors and afterwards determine if any regressor significantly account for the variance found in the BOLD signal. A regressor associated with the measured BOLD signal should hypothetically show a greater value for the voxels in the brain area corresponding to a given task. E.g. finger tapping would show greater β values in the motor cortex. A method for estimating β values for the regressors is the ordinary least squares (OLS). The OLS method estimates β by minimizing the sum of squared residuals [31]:

$$\sum_{i=1}^{n}(Y_i - X_i \times \hat{\beta})^2 \tag{A.14}$$

Y is the observed signal, X is the predicted signal which is scaled by β. β and the variance of β can be estimated by:

$$\hat{\beta} = (X^T X)^{-1} X^T Y \tag{A.15}$$

$$var(\hat{\beta}) = \sigma^2 (X^T X)^{-1} \tag{A.16}$$

The application of this method rests on the following assumptions being fulfilled: Error terms are independently and Gaussian distributed with zero mean, the regressors in the matrix are independent of error, non stochastic and known and no regressor is a linear transformation of another regressor. [31]